

# Characteristics, genesis and parameters controlling the development of a large stratabound HTD body at Matienzo (Ramales Platform, Basque–Cantabrian Basin, northern Spain)



J. Dewit<sup>a,\*</sup>, A. Foubert<sup>a,1</sup>, H.A. El Desouky<sup>a,2</sup>, Ph. Muchez<sup>a</sup>, D. Hunt<sup>b</sup>, F. Vanhaecke<sup>c</sup>, R. Swennen<sup>a</sup>

<sup>a</sup>Earth and Environmental Sciences, KU Leuven, Celestijnenlaan 200E, B-3001 Heverlee, Belgium

<sup>b</sup>Statoil Research Center Bergen, Statoil A.S.A., Sandsliveien 90, 5020 Bergen, Norway

<sup>c</sup>Department of Analytical Chemistry, Ghent University, Krijgslaan 281-S12, B-9000 Ghent, Belgium

## ARTICLE INFO

### Article history:

Received 26 July 2013

Received in revised form

27 December 2013

Accepted 28 December 2013

Available online 8 January 2014

### Keywords:

Stratabound hydrothermal dolomite (HTD)

Reservoir characteristics

Aptian–Albian

Ramales Platform

Basque–Cantabrian Basin

## ABSTRACT

At Matienzo (Basque–Cantabrian Basin, northern Spain), a large stratabound HTD body (4 by 2 km<sup>2</sup> and 80–400 m thick) delimited by two parallel sinistral strike-slip faults is exposed in Aptian carbonates. The margins of the HTD body are characterised by dolomite “tongues” indicating that some limestone beds were more prone to dolomitisation. However, no clear relationship between HTD occurrence and precursor limestone facies can be established. Massive limestone beds, as found at the top of the HTD body, act as barriers to hydrothermal processes, since no dolomite is present in or above these beds. Three types of dolomites have been differentiated, i.e. 1) matrix, 2) coarse crystalline and 3) zebra dolomite. The distribution of the dolomite types is attributed to ascending fluid flow and changing degree of dolomite oversaturation.

The dolomite body was formed by two dolomitisation phases under burial conditions. No indications for a synsedimentary/early diagenetic dolomitisation have been observed. The first dolomitisation phase is characterised by ferroan dolomite and the second by non-ferroan dolomite. The two HTD phases are characterised by depleted  $\delta^{18}\text{O}$ -values (ranging between  $-10\%$  and  $-16\%$  V-PDB),  $\delta^{13}\text{C}$ -values similar to the Aptian–Albian marine signature and homogenisation temperatures of primary fluid inclusions between 120 °C and 150 °C. The dolomitising fluid was enriched in  $^{87}\text{Sr}$  compared to Aptian seawater, excluding the latter as an unmodified fluid source for dolomitisation. Microthermometry of primary fluid inclusions indicates that the dolomitising fluid evolved from a moderate saline (9.7 – 14.0 wt% NaCl) to a more saline (10.9 – 21.0 wt% NaCl) H<sub>2</sub>O–NaCl brine. The dolomitising fluid likely originated from evaporated seawater. Fluid circulation through the dolomitised strata is inferred to have taken place during the tectonically active period of the late Albian throughout which important sinistral-strike slip movements along basement faults occurred.

© 2014 Elsevier Ltd. All rights reserved.

## 1. Introduction

Worldwide hydrothermal dolomites (HTD) have received renewed interest over the last years because of their importance as hydrocarbon reservoirs and/or as zones of increased porosity and

\* Corresponding author. Tel.: +32 16 32 75 80.

E-mail address: [julie.dewit@ees.kuleuven.be](mailto:julie.dewit@ees.kuleuven.be) (J. Dewit).

<sup>1</sup> Present address, Department of Geoscience, University of Fribourg, Chemin du Musée 6, 1700 Fribourg, Switzerland.

<sup>2</sup> Present address: Geology Department, Faculty of Science, Menoufia University, 32512 Shebin El-Kom, Menoufia, Egypt.

permeability (i.e. permeable drains) within carbonate reservoirs (e.g. Cantrell et al., 2004; Davies and Smith, 2006; Dewit et al., 2012). In addition, economic Mississippi Valley-Type (MVT) ore deposits are commonly hosted within HTD (Morrow, 1982; Barnaby and Read, 1992; Malone et al., 1996; Braithwaite and Rizzi, 1997; Hitzman et al., 1998; Boni et al., 2000; Dix and Robinson, 2003; Wilkinson, 2003).

Stratabound HTD bodies, roughly parallel to bedding and occurring in specific strata, can be volumetrically important and represent promising oil and gas reservoirs (Lapponi et al., 2011). Understanding the genesis, geometry and distribution of (reservoir) characteristics of stratabound HTD bodies is therefore essential to evaluate and predict their reservoir potential.

The origin of large HTD bodies and the nature of the dolomitising fluid is a matter of debate. Large HTD bodies are often interpreted as the result of “cannibalism” or in other words of overprinting of a syndimentary/early diagenetic dolomite to overcome Mg mass balance issues. In some cases, clear evidence for early and late diagenetic dolomites can be found (e.g. Gao et al., 1992; Malone et al., 1996; Cantrell et al., 2004; Sharp et al., 2010), however, this is not always the case (e.g. Barnaby and Read, 1992; Gasparrini et al., 2006).

In order to evaluate the dimensions of HTD bodies in the subsurface, it is crucial to know which parameters control the extent of hydrothermal dolomitisation. Since HTD bodies are most often related to faults, tectonic structures have to be considered as potential controlling parameters. In addition, the influence of the precursor limestone host rock has to be considered as well since HTD locally occur in “tongues”, i.e. replacing specific horizons, and thick limestone units or other impermeable beds cap the HTD body.

Dolomitisation can result in destroyed, maintained or enhanced porosity compared to the limestone host rock (Negra et al., 1994; Sun, 1995). Moreover, the reorganisation of the pore network affects the permeability of the dolomitised rock, usually in a positive way (Warren, 2000). Nevertheless, the general effect of hydrothermal dolomitisation on reservoir properties is matter of debate since degraded reservoir properties as a result of hydrothermal dolomitisation have been encountered too. In general, the range of porosity and permeability values and the distribution of these petrophysical characteristics in subsurface HTD reservoirs are largely unknown. Therefore, reservoir analogue studies can provide key information to predict the reservoir characteristics and their distribution in the subsurface. The range of porosity and permeability values of the Matienzo HTD body, as well as the distribution of these characteristics, form the base to assess the reservoir potential of a stratabound HTD body. The Matienzo HTD body represents an excellent reservoir analogue for the hydrocarbon reservoirs hosted by stratabound HTDs, e.g. producing hydrocarbon reservoirs of the Middle Ordovician Albion Scopio trend and Stoney Point field (Michigan Basin, USA). The Matienzo HTD body and Albion Scopio trend and Stoney Point field reservoirs share many characteristics in terms of tectonic setting and geometry. For instance, the latter hydrocarbon reservoirs consist of HTD bodies bounded by subparallel wrench faults, are 1.6 km and 3–39 km long and are laterally sealed by the impermeable host rocks (of the Trenton and Black River Formations) (Grammer and Harrison, 2013).

In this contribution, the results of the study of a large stratabound HTD body hosted by the Ramales Platform (Basque–Cantabrian Basin, northern Spain) are presented and discussed in terms of, geometry, reservoir characteristics and genesis.

## 2. Geological setting

The study area is situated in the west of the Basque–Cantabrian Basin (BCB), northern Spain (Fig. 1 A). This extensional basin originated in the Triassic and evolved from a rifting to a spreading basin during the Cretaceous. From the late Cretaceous onwards, it was influenced by the Pyrenean Orogeny. Inversion of the basin only started in the Miocene (Rat, 1988; Boillot and Malod, 1988; Vergés et al., 2002; Sibuet et al., 2004).

The extension of the BCB is related to the opening of the North Atlantic Ocean and the Bay of Biscay. The most important phase of extension and subsidence of the basin took place during the Aptian and Albian (García-Mondéjar, 1989; García-Mondéjar et al., 1996, 2005). This subsidence was coeval with a global sea-level rise, resulting in the connection of the BCB with the Tethys and the influx of warm waters (Martín-Chivelet et al., 2002). Syndimentary tectonic activity and differential subsidence along NW–SE and NE–SW faults resulted in structural highs, on which carbonate platforms formed, and intra-platform troughs, in which thick successions of basinal sediments were deposited. The Aptian–Albian shallow-water platform carbonates of the BCB are typically characterised by a tight micritic facies with rudists, chondrodonta and orbitolionids (i.e. an Urgonian facies) (Fernández-Mendiola and García-Mondéjar, 1990).

The largest carbonate platform developed in the BCB is the Ramales Platform (Fig. 1 B). In this platform, most HTD is observed in Albian carbonates of the Ramales Formation, i.e. in the areas of Ranero and Bueas (López-Horgue et al., 2010; Shah et al., 2010; Swennen et al., 2012; Dewit et al., 2012). The study area is situated 10 km NW of Ramales de la Victoria, adjacent to the village of Matienzo (Fig. 2). The HTD body exposed at Matienzo is hosted by ramp carbonates dated as Gargasian and Clanayes (Aptian stages) and early Albian (García-Mondéjar, 1990).

The study area is bounded by two sub-parallel sinistral strike-slip faults, the Seldesuto Fault and the Matienzo Fault (Figs. 2 and 3 A). These faults are part of a large scale sinistral wrench zone, developed between the Cabuérniga and the Bilbao Faults. The latter faults respectively run north and south of the study area (Gómez et al., 2002). The Bilbao Fault has a north-west strike, while the Cabuérniga Fault runs east-west from Ramales de la Victoria to the

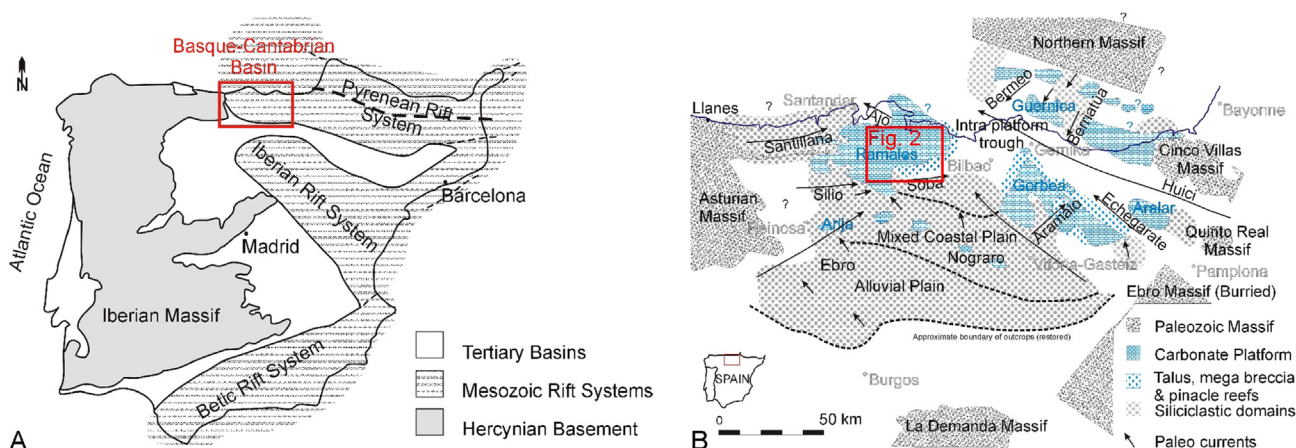


**Figure 1.** A. The Basque–Cantabrian Basin is part of the western extension of the Pyrenees (after Grandia et al., 2003). B. Sedimentary domains during the Aptian–Albian in the Basque–Cantabrian Basin (after García-Mondéjar, 1982).

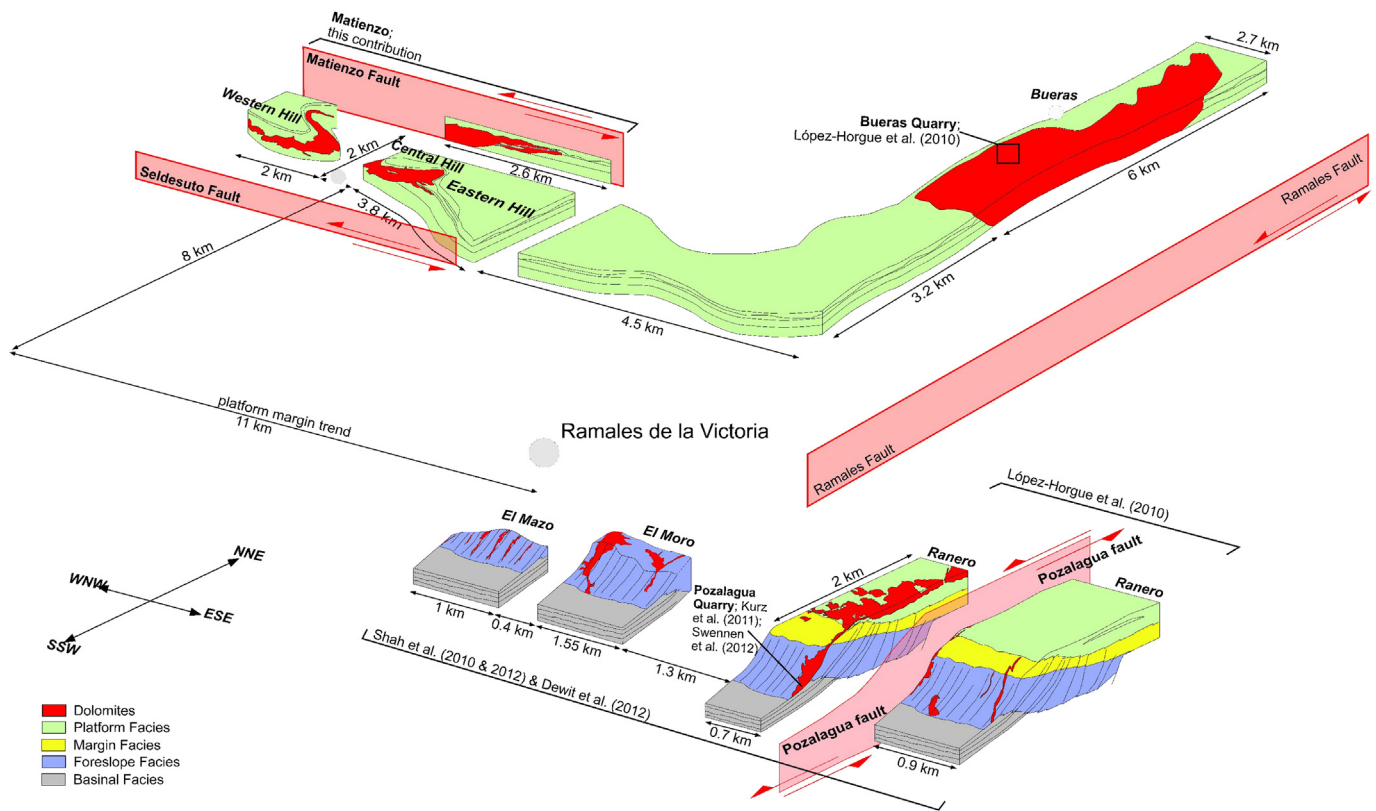


**Figure 2.** Sketch showing the occurrence of HTD bodies in the southern part of the Ramales Platform (margin and inner platform), the most important faults and previous studies.

Cantabrian Mountains. The nature of the Cabuérniga Fault changes from a sinistral strike-slip fault in the study area to a thrust fault reactivated during the Alpine Orogeny in the Cantabrian Mountains (Alonso et al., 1996). The north-south oriented step-over Ramales Fault developed between these two regionally important faults (García-Mondéjar et al., 1996). The genesis of different HTD bodies of the Ramales Platform has been related to the activity of the Ramales fault (López-Horgue et al., 2010).

In the Ramales Platform, several HTD bodies occur in Aptian and Albian carbonates (Fig. 2), which are characterised by similar paragenetic sequences (Dewit, 2012). These HTD have been studied by a number of authors, however, these studies are focused on the small HTD bodies occurring along the Ramales Platform margin (López-Horgue et al., 2010; Shah et al., 2010, 2012; Dewit et al., 2012) or exposed in the Pozalagua Quarry (López-Horgue et al., 2010; Kurz et al., 2011; Swennen et al., 2012) (Fig. 2). López-Horgue et al. (2010) also studied the genesis of the HTD the stratabound HTD body exposed at the Bueras Quarry (Fig. 1) and demonstrated the hydrothermal nature of the dolomites hosted by the Ramales Platform by comparing fluid inclusion microthermometry data with the burial curve. The maximum burial temperature of the Ramales Platform is estimated at 75–90 °C at the moment of dolomitisation, while the measured homogenisation temperatures of fluid inclusions in the HTD are around 120 °C or higher (López-Horgue et al., 2010). Based on field observations and the late Cretaceous tectonic activity climax, the timing of the dolomitisation can be inferred as Late Albian-Cenomanian (López-Horgue et al., 2010; Swennen et al., 2012). The reservoir characteristics of HTD bodies cropping out along the Ramales Platform margin are studied by Dewit et al. (2012), however, in the reported case the HTD bodies are small and fault-controlled compared with the large and

stratabound HTD body discussed in this contribution (Fig. 2). Studying stratabound HTD bodies allows understanding additional controls, such as primary lithology, on the distribution of HTD and its petrophysical characteristics.

### 3. Methods

The areal extent of the HTD body was assessed with a Digital Outcrop Model (DOM) and ground-truthed by field work. Two sedimentological sections were described in detail and sampled to analyse the limestone facies and dolomite distribution at Matienzo (Fig. 3). The HTD were extensively studied and sampled laterally from the lithological sections to obtain a good insight in the extent of the HTD body, the dolomite-limestone contact, the distribution of the HTD types and HTDs' characteristics. After staining the hand specimens for investigation of the mineralogy using Alizarin Red S and potassium ferricyanide (Dickson, 1966), thin-sections were selected to study sedimentary textures and diagenetic products. In total, 75 thin-sections of the limestone host rock and HTD were analysed with standard petrographic methods (transmitted light and cold cathode luminescence microscopy).

Powder samples were drilled out with a dental drill for stable C–O and radiogenic Rb–Sr isotopic analysis. C and O isotope ratios were determined at the University of Erlangen (Germany). Carbonate powders were reacted with 100% phosphoric acid (density >1.9; Wachter and Hayes, 1985) at 75 °C using a Kiel III online carbonate preparation line connected to a Thermo Finnigan 252 mass spectrometer. All values are reported in per mil relative to V-PDB by assigning a  $\delta^{13}\text{C}$  value of +1.95‰ and a  $\delta^{18}\text{O}$  value of –2.20‰ to NBS19. Oxygen isotopic compositions of dolomite were corrected using the fractionation factors given by Rosenbaum and Sheppard (1986).

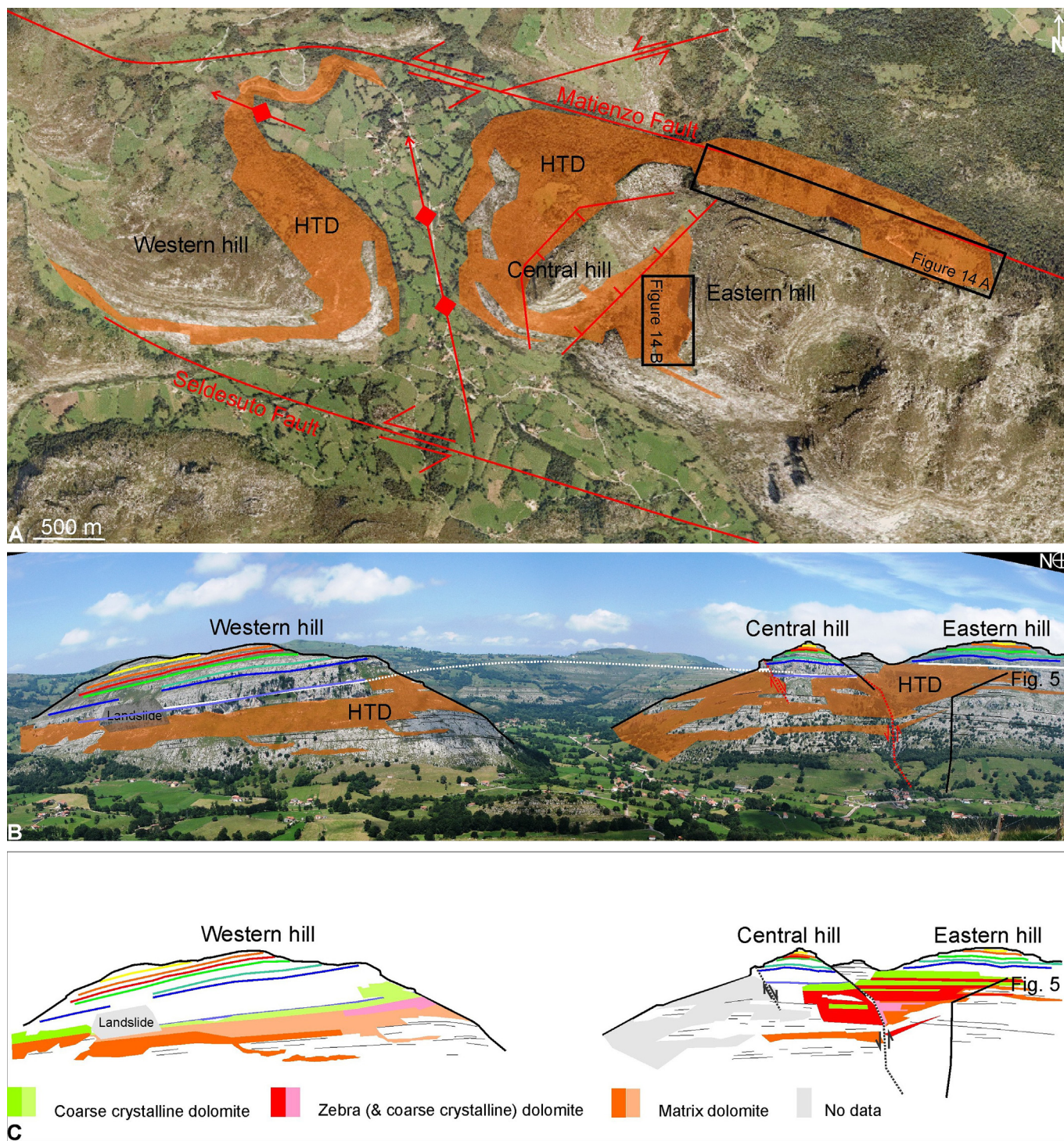


**Figure 3.** A. Map view of the structural setting of Matienzo. The HTD body is indicated in orange. Black rectangles show the areas where plugs were collected for standard porosity and permeability measurements. B. View on the southern part of the Matienzo outcrops. The HTD body (orange) is a large stratabound body. The black line indicates the location of the lithological section shown in Figure 5. The top of the HTD body is bounded by a massive limestone layer (base indicated with a white line). C. Overview of the HTD type distribution in the HTD body of Matienzo. The shaded colours represent the zones where the HTD type distribution is based on a limited number of observations due to limited exposure conditions.

The Rb–Sr analyses were performed at the Department of Analytical Chemistry, Ghent University (Belgium). Carbonate powders were weighed and dissolved in 6 M HCl on a hotplate. The digests were subsequently evaporated to dryness and redissolved in 7 M HNO<sub>3</sub>. The elemental Rb and Sr concentrations were determined using a Thermo Scientific XSeries 2 quadrupole-based

ICP-MS instrument; external correction was relied on for quantification, while Y was used as internal standard, correcting for matrix effects and signal instability. The <sup>87</sup>Rb/<sup>86</sup>Sr ratios were calculated following the procedures described by Vanhaecke et al. (1999). Sr was isolated from the sample matrix using a Sr spec™ resin, following the isolation procedure of De Muyck et al. (2009). Sr

isotope ratio measurements were performed using a Thermo Scientific Neptune multi-collector (MC) ICP-MS instrument. The intensities obtained for  $^{83}\text{Kr}$  and  $^{85}\text{Rb}$  were used to correct for the Kr and Rb interferences. The Sr isotope ratios were normalised to the accepted  $^{86}\text{Sr}/^{88}\text{Sr}$  ratio of 0.1194. Blank Sr signals were negligible compared to the Sr intensities encountered for samples and standards. Repeated analyses of NIST SRM 987  $\text{SrCO}_3$  over the duration of this study yielded an average  $^{87}\text{Sr}/^{86}\text{Sr}$  ratio of  $0.710296 \pm 0.000033$  ( $n = 43$ ), in agreement with the accepted  $^{87}\text{Sr}/^{86}\text{Sr}$  ratio of 0.710248 for this material (Thirlwall, 1991).

A fluid inclusion microthermometric study was performed on three representative double polished wafers ( $\sim 100 \mu\text{m}$  thick). Measurements were done on Linkam THMSG-600 and Linkam MDS-600 heating-freezing stages mounted on Olympus BX60 and Olympus BX51 microscopes, respectively. The stages were calibrated by synthetic Syn Fliac fluid inclusion standards. Reproducibility was better than  $0.2^\circ\text{C}$  for the first (Tfm) and final ice melting ( $T_{\text{mice}}$ ) temperatures and within  $3^\circ\text{C}$  for the liquid–vapour homogenisation temperatures (Th). Fluid inclusions selected for microthermometry were carefully chosen after petrographic investigation of the wafers. Primary aqueous two-phase (L + V) fluid inclusions with a consistent liquid–vapour ratio ( $\sim 10\%$ ) and regular shape were observed in growth zones parallel to crystallographic orientations. Salinities are reported in equivalent weight percent NaCl (eq. wt% NaCl) and were calculated based on the equation of Bodnar (1993).

Standard helium porosity and Klinkenberg permeability measurements were performed on 55 plugs at CoreLab. The plugs have a diameter of 2.5 cm and minimum length of 5 cm. Helium porosity measurements rely on Boyle's Law. Permeability measurements were carried out with  $\text{N}_2$  gas under a series of pressure conditions in order to determine the standard Klinkenberg permeability.

## 4. Results

### 4.1. Field and petrographic observations

Exposures of the Matienzo HTD body are spread over the “Western”, “Central” and “Eastern Hill” adjacent to Matienzo village (Fig. 3). In these outcrops, Aptian carbonates host the stratabound HTD body. The Digital Outcrop Model (DOM) of the area allows identification and tracking of specific strata throughout the study area. Different layers can be followed from the Western to Central and Eastern Hill (Fig. 3 B). The gradually changing strike and dip indicate that the strata are gently folded and form an anticline. The sequence of (dolomitised) strata observed between the two sinistral faults can not be observed north of the Matienzo or south of the

Seldesuto Fault. The well-bedded character of the limestone beds occurring north and south of these faults suggests they correspond to younger Albian inner-platform deposits. Therefore, normal faulting occurred along the Matienzo and Seldesuto Faults during the sinistral strike-slip regime and/or during the Alpine deformation. Even though there is a geometric relation between the HTD body and the sinistral strike-slip faults, no indications for a genetic relation between the faults and the HTD emplacement could be observed, with the exception of dolomite-cemented shear veins.

The dolomite–limestone contact can be observed in the DOM and was systematically ground-truthed during extensive field work. The dolomite occurrence is highlighted in Figure 4; in general, areas covered with grass correspond to dolomite. Limestone layers are more resistant to weathering and can be recognised as grey, bedded strata. The HTD body is tabular (4 km long, 2 km wide), between 80 and 400 m thick and roughly respects the orientation of the bedding. The outline of the HTD body is characterised by the following dominant features: 1) the top of the HTD body is generally flat and occurs under a massive limestone unit (Fig. 3), 2) the HTD body pinches out laterally and several “tongues” of dolomite can be observed in the eastern extremity (Fig. 4 A), 3) some limestone beds virtually unaffected by the dolomitisation, referred to as “stringers”, are present within the HTD body (Fig. 4 B), 4) fractures locally control the dolomite–limestone contact (Fig. 4 C), 5) rudist and oyster buildups occurring below the main HTD body are generally selectively dolomitised (Fig. 4 D).

#### 4.1.1. Host rock

To characterise the limestone host rock and the relation between precursor limestone facies and dolomite, sections were logged in the Eastern Hill and in the lower part of the Central Hill. Three major units are distinguished within the Aptian succession (Figs. 3 B, C and 5).

The base of unit 1 consists of dolomite-cemented mica-rich sandstones with shale intercalations, probably corresponding to the top of the Arroyo Formation, which is described by Robador Moreno et al. (2000) as sandy limestone and sandstone and occurring below the Ramales Formation. Above the sandstone succession, fine-grained, clay-rich limestones are intercalated with shales. Bioclasts present in the limestone are crinoids and brachiopods. Shale beds gradually become thinner and finally disappear, until only clay seams can be observed between limestone beds. In the lower part of the section, which is generally dominated by siliciclastics, a thick bed ( $\pm 1 \text{ m}$ ) with large rudists is present (Fig. 6 A) that serves as a marker horizon. A 5 m-thick limestone bed with irregular chert nodules is observed in the different hills at Matienzo and also serves as a good marker horizon (Fig. 6 B). This

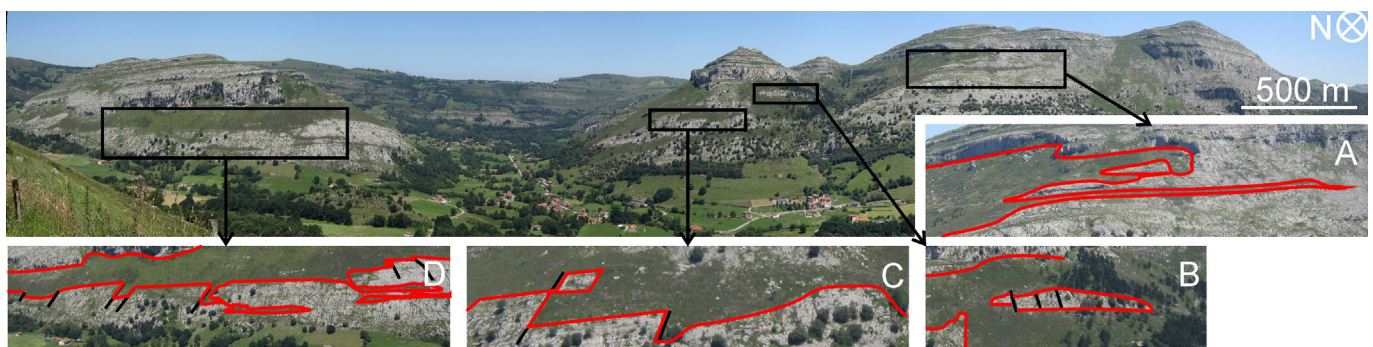


**Figure 4.** Outline of the stratabound HTD body at Matienzo. A. Dolomite “tongues” occur in the lateral extremities of the HTD body. B. Limestone “stringers” are present within the HTD body. C. Fractures locally control the dolomite–limestone contact. D. Rudist buildup occurring just below the main HTD can be dolomitised. The dolomite–limestone contact is highlighted by a red line and fractures by black lines. (For interpretation of the references to colour in this figure legend, the reader is referred to the web version of this article.)

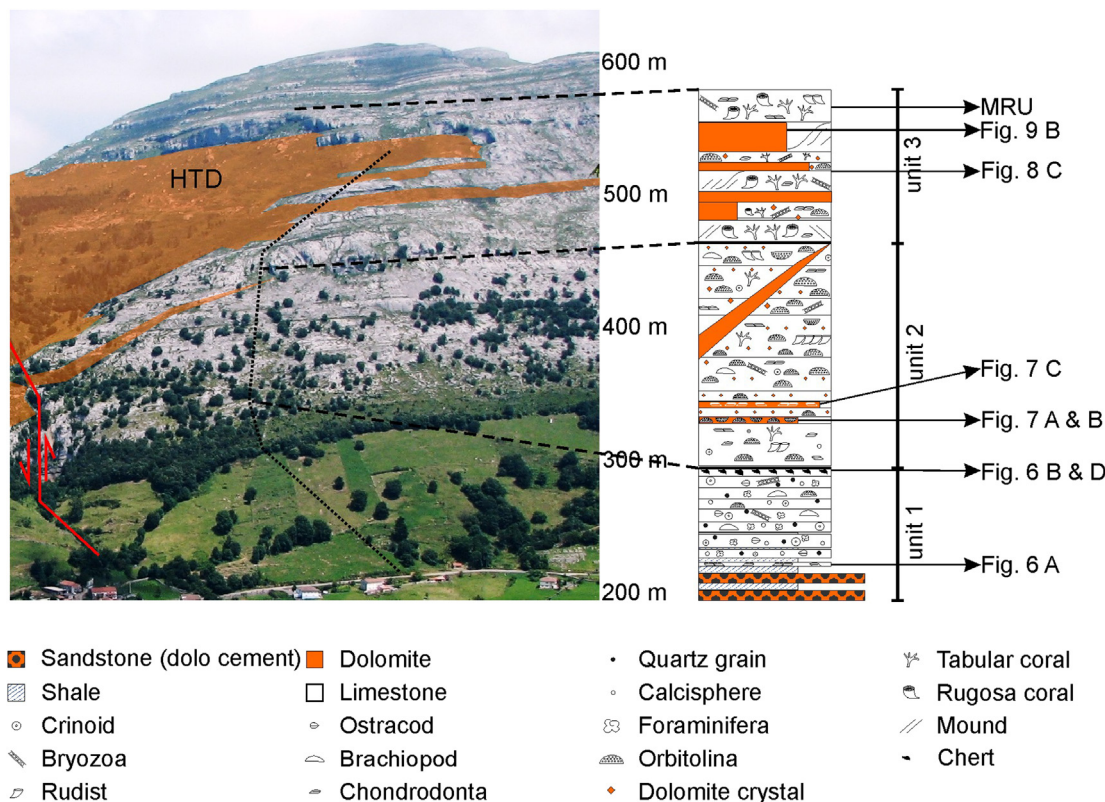


Figure 5. Photograph and lithological log of the three limestone units observed at Matienzo (Eastern Hill). MRU = Matienzo Reference Unit.

chert-rich layer is defined as the upper boundary of the first limestone unit.

Macroscopically, no dolomite has been observed in the clay-rich limestones. These mudstones to wackestones contain sub-rounded quartz grains with a relatively uniform grain size (50–200 μm) and different bioclasts, i.e. crinoids, foraminifera (orbitolinid), ostracoda, calcispheres, brachiopod shells and bryozoa fragments. Stained thin-sections reveal that some bioclasts have been replaced by ferroan dolomite (Fig. 6 C). Pyrite occurs locally in association with this dolomite. The chert-rich marker horizon consists of foraminifera (e.g. miliolid), calcified sponge spicules and quartz grains in a (locally silicified) micrite matrix (Fig. 6 D). In general, the bioclasts and matrix of unit 1 have a distinct luminescence. The matrix is characterised by a dull orange luminescence, while bioclasts can display different hues of luminescence ranging from non-luminescent to bright luminescent (Fig. 6 E and F).

Unit 2 starts with thick-bedded limestones. Brachiopods are less common, while chondrodonta and rudists are omnipresent, first as solitary shells and subsequently composing in situ colonies. The first dolomite occurrences consist of fine crystalline, partially dolomitised strata. The weathered surface accentuates the casts of orbitolinids that remain unaffected by dolomitisation (Fig. 7 A and B). The second substantial dolomite occurrence (1.5 m thick and 5 m long) is present in an oyster buildup. The dolomite is fine crystalline and replaces the matrix around the shells, while the bioclasts are remarkably well preserved (Fig. 7 C). This dolomite is underlain by limestone beds, in which large dolomite crystals (~1 mm) occur dispersed in the matrix and around bioclasts. Higher upward, the limestone beds become bioclast-rich and are partially dolomitised to different degrees, limestone beds without dolomite are scarce.

Above the partially dolomitised bioclast-rich beds, thick-bedded limestones occur (Fig. 5). They consist of bioclastic wackestones and

packstone with orbitolinids being omnipresent. Bioclasts and matrix are both non-luminescent. Partial dolomitisation is frequently observed in these limestones. The dolomitisation is fabric-selective, the micrite matrix and calcite-cemented vugs are preferentially dolomitised (Fig. 7 D), while bioclasts (orbitolinids, crinoids, coral fragments, ...) are not affected (Fig. 7 E). In the case of rudists and brachiopods, the inner shell is preferentially dolomitised (Fig. 7 F). The dolomite crystals are characterised by anhedral crystal shapes, sweeping extinction, a lot of impurities (except for their outer rim), and show a general dull red luminescent core and a bright luminescent outer rim.

In the Eastern hill a first large, coarse crystalline dolomite body cross cuts the unit 2 strata (Fig. 5). This subsidiary not-stratabound dolomite body, which can be followed over 350 m and has a variable width, starts at the fault separating the Central and Eastern Hill and runs parallel to a dolomite vein and fracture orientation of N60W80N. The latter broadly coincides with a main fracture set observed in the area. The fracture-controlled body is at its largest width in the vicinity of the fault (~20 m). The width gradually decreases eastwards, where the body finally pinches out. The outlines of primary bioclasts can be observed locally in the dolomite.

At its base, unit 3 consists of a 7 m-thick, massive, relatively homogeneous limestone layer. Tabular and solitary corals are the dominating bioclasts. Subsequently, thick, massive limestone layers (~10 m thick) characterised by mound features (i.e. foresets, corals and rudists colonies, Fig. 8 A) occur between thinner beds. Locally, coarse crystalline dolomite replaces the limestone host rock, resulting in different dolomite “tongues” (Figs. 3, 4 A and 5). These dolomite tongues represent the eastern extremities of the large dolomite body occurring at Matienzo.

In thin beds, bioclasts like corals, gastropoda and rudists are preferentially dolomitised (Fig. 8 B). Thick, massive limestone layers are the least dolomitised. The upper dolomite-limestone

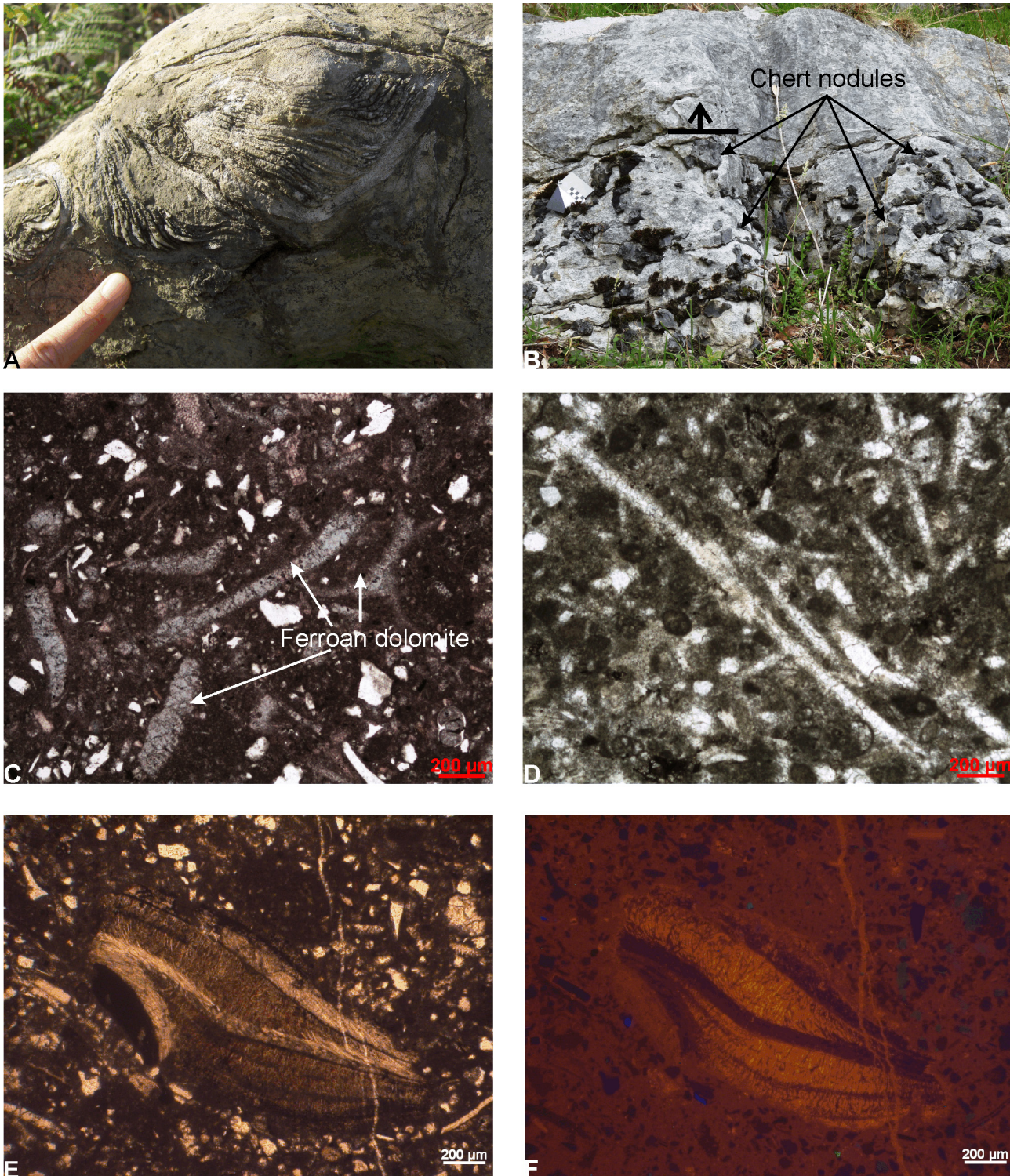


**Figure 6.** A. Limestone rich in large rudists serves as a marker bed at Matienzo. B. Limestone with irregular chert nodules at the top of unit 1. C. Fabric-selective ferroan dolomite (blue stain) in a quartz-bearing limestone of unit 1. D. Calcified sponge spicules in a chert-rich limestone bed. E & F. Optical and equivalent cathode luminescence microphotographs. In unit 1, limestones, matrix and bioclasts display a different luminescence in contrast to the limestones of unit 2 and 3. (For interpretation of the references to colour in this figure legend, the reader is referred to the web version of this article.)

contact occurs below such a massive limestone unit, which is composed of bioclastic wackestones alternating with nodular limestone beds. It is defined as a third reference unit, the Matienzo reference unit (MRU). Unit 3 limestones are dolomitised to different degrees. The texture of the limestones is ranging from bioclastic

mudstones to grainstones. However, no relation between the limestone fabric and the degree of dolomitisation could be established based on field and thin-section investigations. The partial dolomitisation of unit 3 limestones is always fabric-destructive and -selective, i.e. dolomite occurs preferentially around large bioclasts,

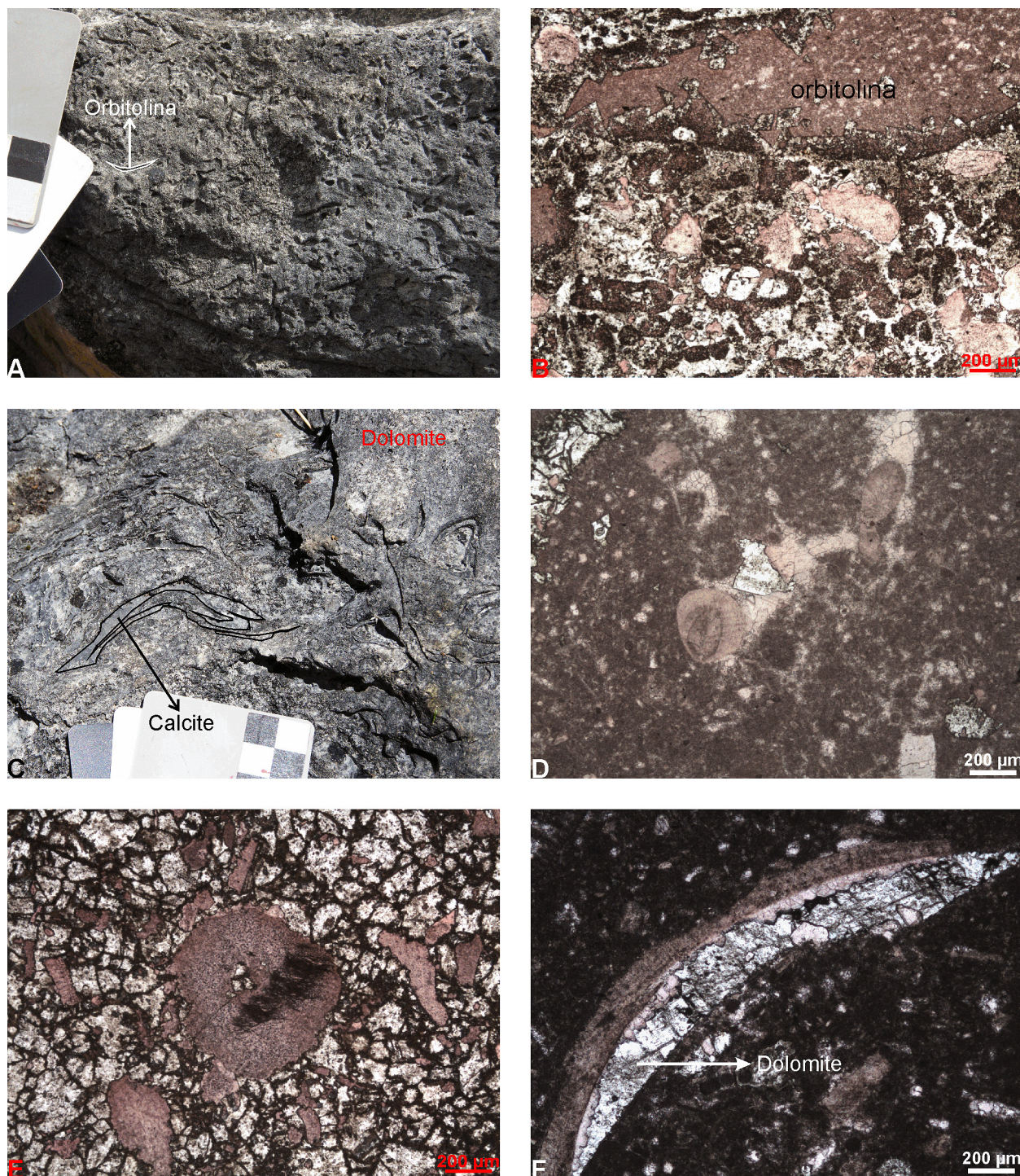


**Figure 7.** A. Partially dolomitised limestone. The weathered surface accentuates the outline of the non-dolomitised orbitolinids. B. Partially dolomitised orbitolinid-rich bed. The stained thin section nicely reveals the preservation of the orbitolinids (and other bioclasts). C. Dolomite in an oyster-rich limestone bed. The matrix has been dolomitised, while oyster shells remain well preserved. D. Partially dolomitised limestone with dolomite preferentially replacing calcite in small vugs. E. Example of fabric-destructive, but selective dolomitisation. Crinoids remain unaffected by dolomitisation. F. Dolomite preferentially affecting (and locally replacing) the inner shell of brachiopoda.

replaces bioclasts and calcite cement in irregular vugs and is finely dispersed in the matrix. The matrix and bioclasts are, in general, non-luminescent, whereas dolomite crystals appear as a dull to bright red luminescent.

In the three sedimentary limestone units, primary porosity was low and early diagenetic cements resulted in the occlusion of primary pores in the limestone host rock. All early diagenetic cements are composed of small ( $\leq 100 \mu\text{m}$ ) blocky calcite crystals. This

calcite cement can be distinguished from the two calcite generations post-dating dolomitisation since it is cross cut by stylolites and dolomite-cemented veins.

#### 4.1.2. Dolomite

Most of the dolomite occurs within unit 3 limestones under the MRU. The large HTD body is generally bed-parallel and developed in specific strata (Figs. 3 and 8 C). The body is therefore stratobound.



**Figure 8.** A. Foresets of mounds in massive limestone beds. B. Bioclasts in thin limestone beds are preferentially dolomitised. C. Bedding-controlled dolomite-limestone contact. D. Preserved coral texture in dolomite.

Several dolomite tongues can be observed in the Eastern Hill (Figs. 3, 4 A and 5), suggesting that some limestone beds were more prone to dolomitisation than others, although no obvious relation between the precursor limestone facies and the dolomite occurrence was observed. These tongues can be up to 400 m long and stop at the contact with a massive limestone layer or mound. The limestone beds above and below the dolomite tongues are partially dolomitised, with a gradual transition ( $\sim 0.5$  m) at the limestone-dolomite contact. The massive limestone layers occurring laterally to the dolomite tongue contain little or no dolomite. Within the dolomitised layers, the outline of bioclasts (e.g. corals) can be recognised locally (Fig. 8 D).

The HTD are characterised by three main textures, i.e. 1) dark grey, fine crystalline matrix dolomite, 2) white-pink, massive coarse crystalline dolomite, and 3) zebra dolomite (Fig. 9 A and B). Matrix dolomite is made of non-planar crystals containing many impurities. The average crystal size of matrix dolomite is  $200 \mu\text{m}$  (Fig. 9 C and D). Coarse crystalline dolomites are characterised by large crystals ( $\geq 1000 \mu\text{m}$ ) with sweeping extinction and a brownish colour due to a concentration of small inclusions and impurities (Fig. 9 E and F). These crystals are fringed by a limpid rim with a distinct bright luminescence compared to the general dull luminescence of the crystal centres (Fig. 9 G and H). Zebra dolomites are built up by alternating layers of small crystals, like those

characteristic for the matrix dolomites (A-band), and large crystals, like those characteristic for coarse crystalline dolomites (B-bands). Zebra dolomite consists of ABBA-bands with gradual transition between both, as described by Nielsen et al. (1998) and Vandeginste et al. (2005).

A section on the northern flank of the Eastern Matienzo Hill offers a good overview of the lateral and vertical distribution of HTD types (i.e. matrix, zebra and coarse crystalline dolomite). The occurrence of the HTD as shown in Figure 3 C is based on mapping by means of a digital outcrop model (DOM) and field ground-thruthing. The top of the dolomite body seems to be controlled by the thick Matienzo reference unit (MRU; Fig. 3), above which only small patches of dolomite can be found sporadically. In the lower part of the HTD body, matrix dolomite dominates. Isolated layers of zebra dolomite occur sporadically. The middle part of the HTD body consists mainly of zebra dolomite with millimeter to centimeter large pores parallel to the typical ABBA-bands of zebra dolomites. The zebra dolomites are frequently occurring in horizons of  $\sim 30$ – $50$  cm thick, which are separated by horizons of relatively coarse crystalline matrix dolomite. Dolomite tongues occurring in the middle part of the HTD body are generally made of matrix dolomite, though locally zebra dolomites are observed. The upper part of the dolomite body under the MRU is characterised by coarse crystalline (and zebra) dolomites with aligned or irregular

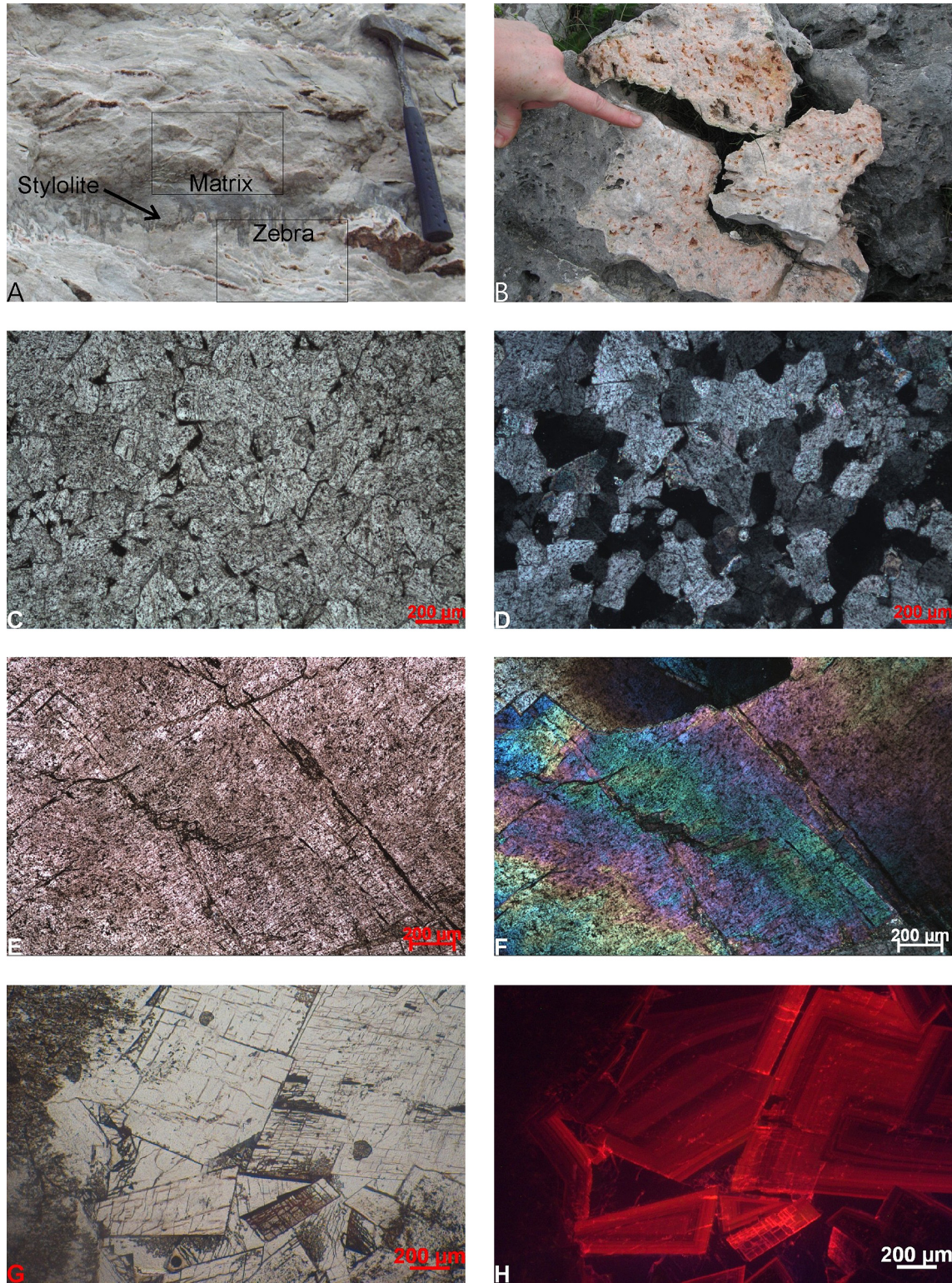


**Figure 9.** A. Matrix and zebra dolomite. B. Coarse crystalline dolomite. C & D. Corresponding microphotographs with parallel and crossed polars of small, anhedral dolomite crystals. E & F. Corresponding microphotographs with parallel and crossed polars of large dolomite crystals with sweeping extinction. G & H. Transmitted and corresponding cathode luminescence microphotograph. Coarse dolomite crystals are limpid and characterised by a bright red, sometimes intensely zoned, luminescence. (For interpretation of the references to colour in this figure legend, the reader is referred to the web version of this article.)

vugs. The particularity of these upper 80 m of the HTD body is the occurrence of coarse crystalline dolomite with large vuggy pores (Fig. 10 A). The pores have an irregular shape and can be up to 12 cm long and 2 cm wide. Based on computer tomography data analysis,

porosity in these top 80 m of the HTD body was found to be ~11% (Fig. 10 B). In addition, in the upper 5 m below the dolomite-limestone contact a gradual transition to the limestone host rock can be observed first by the occurrence of moldic pores in coarse

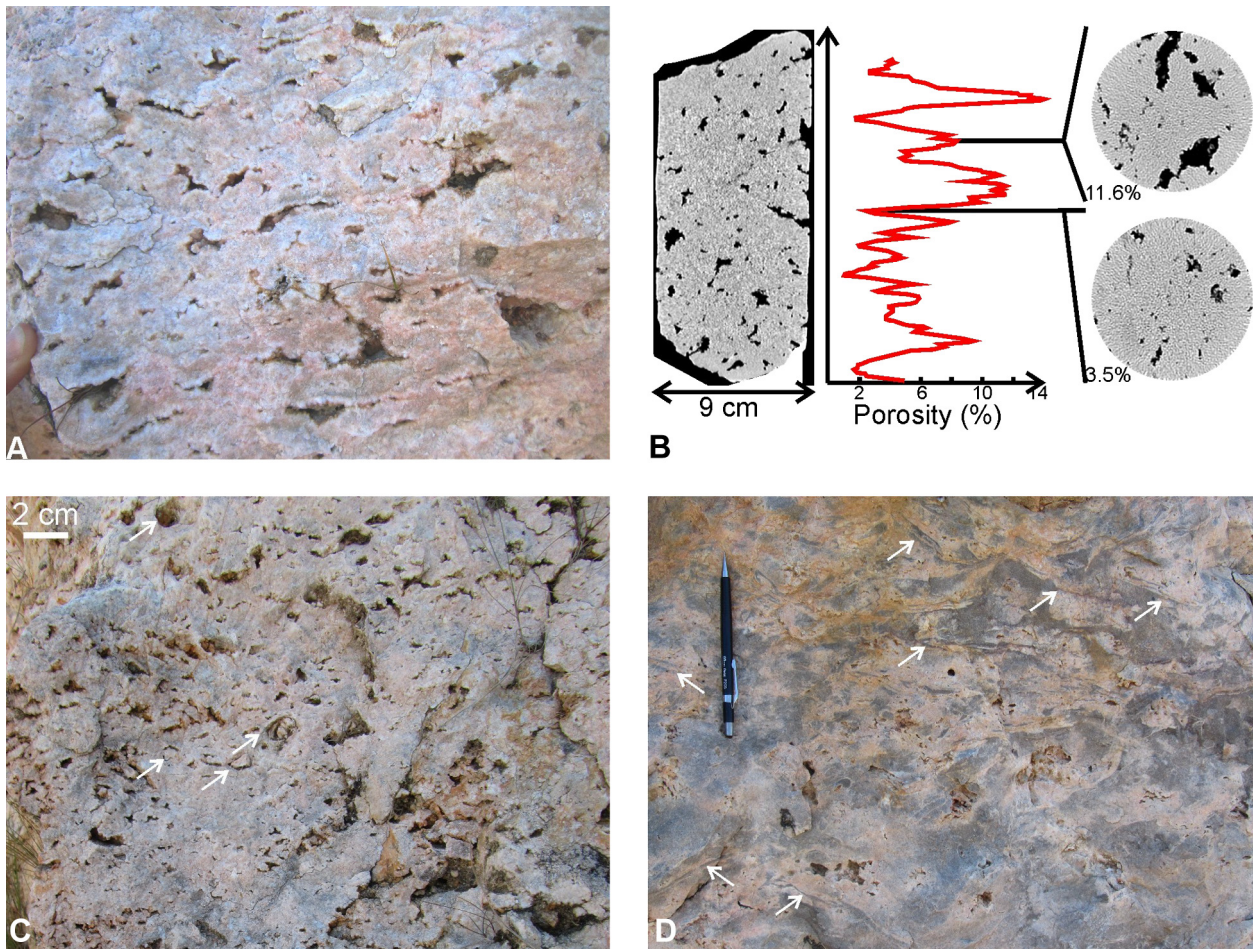


**Figure 10.** A. Coarse crystalline dolomites with large vuggy pores exposed near the upper dolomite-limestone contact. B Computer tomography (CT) data of a large core (9 cm diameter) of dolomite shown in A. Based on CT data analysis, the porosity of the large core was estimated at 11%. Porosity distribution varies within the large as shown by the porosity distribution curve along the axis of the core and two slices perpendicular to the axis of the core. C. Coarse crystalline dolomite with moldic pores. Some rudist cast pores are indicated by white arrows. D. Mixed coarse and fine crystalline dolomite with chondrodonta outlines (white arrows).

crystalline dolomite (Fig. 10 C) and subsequently by the preservation bioclast outlines in dolomite consisting of coarse and fine crystalline dolomite (Fig. 10 D).

The MRU that caps the (highly porous) top of the HTD body at Matienzo is cross cut by a fault-bound “horst” structure in the Central Hill (Fig. 11 A). The horst structure has a general N30W strike. One large normal fault defines the southern margin of the horst and two small faults are observed at the northern border of the horst. The offset by the normal faults is important at the base of the structure, where it reaches up to 8 m (Fig. 11 A). The two small faults offset the MRU over 1 and 4 m, respectively, as highlighted in yellow in Figure 11 A and B. In the horst structure, dolomite affects the limestone layers above the MRU (Fig. 11 C). The upper part of the horst is characterised by a fault displacement of ~3 m (Fig. 11 A). At this point, almost no dolomite can be observed. Finally, fault propagation diminishes over the following 10 m, where the limestone layers are no longer offset (pink limestone layer; Fig. 11 A). In the prolongation of the horst structure, closely spaced, dolomite-cemented veins (N45W90) are present. Similar faults can be observed on field photographs, but were not investigated during field work (dotted lines, Fig. 11 A).

Based on cutting relations in stained massive dolomite samples, two phases of dolomitisation can be differentiated. The first dolomite generation consists of ferroan and the second of non-ferroan dolomite. Both dolomite phases occur as matrix, zebra and coarse

crystalline dolomite textures. No difference in luminescence is observed for ferroan and non-ferroan dolomites, they are generally dull red luminescent. The HTD are all pre- and post-dated by sub-horizontal stylolites, which was also observed by Swennen et al. (2012). Along some of the stylolites, dolomite rhombs can be observed, indicating that the latter served as a fluid conduit and developed prior to dolomitisation.

#### 4.1.3. Calcite post-dating dolomite

Based on cross cutting relations, two calcite phases post-dating dolomitisation can be observed in the study area, i.e. blocky calcite and honey calcite. The first calcite phase occurs in veins and cavities and is made of white to translucent blocky crystals. The second calcite phase is characterised by honey-coloured to transparent crystals and is associated with alteration rims and iron oxides. It also occurs as columnar crystals arranged in rosettes and speleothems.

The first calcite phase consisting of blocky crystals is usually non-luminescent, though in some rare cases it contains zones with a dull luminescence. It is characterized by the presence of intense cleavage with type II twins (Burkhard, 1993). The second calcite phase virtually has no cleavage twins, is non-luminescent, but locally a zoned dull or bright luminescence can be observed (Fig. 12 A and B). Macroscopically, dolomites in contact with the honey-coloured calcite often show a pink or brown hue. In

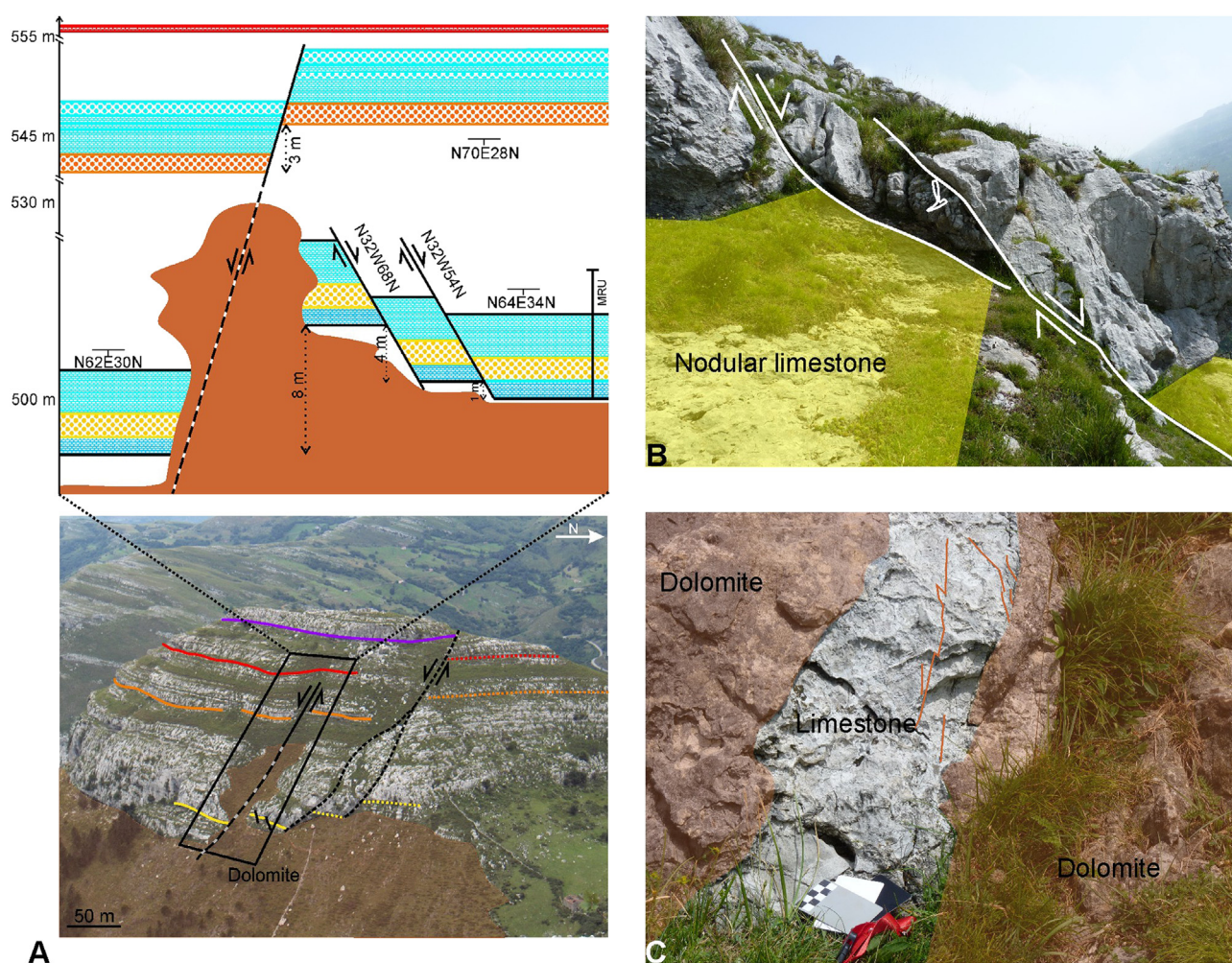


**Figure 11.** A. Sketch and photograph of the horst structure in the Central Hill at Matienzo. In the sketch and photograph, (nodular) limestone layers traceable across or above the horst are highlighted in yellow, orange and red. The dolomite body intruding the limestones along the horst structure is shown in brown. B. Normal faults displacing a nodular and thick limestone layer in the northern part of the horst structure (hammer for scale). C. Dolomite intruding the younger limestones on top of the MRU in the horst. (For interpretation of the references to colour in this figure legend, the reader is referred to the web version of this article.)

general, a corroded surface marks the contact between the dolomite crystals and the honey-coloured calcite. The corrosion can be accompanied by the development of intra-crystalline porosity and crystallisation of iron (hydr)oxides. Locally, the cast of these dolomite rhombs is now filled with the second calcite phase (Fig. 12 C and D). Therefore, the dolomite crystals must have been (partially) dissolved and subsequently replaced by this calcite phase (i.e. dedolomitisation).

#### 4.2. Reservoir characteristics

Petrophysical characteristics were measured on 55 dolomite plug samples taken in the Western Hill and in the southern and northern face of the Eastern Hill (Fig. 3 A). Since the limestone host rock was tight, no samples have been analysed for standard porosity and permeability. When selecting the plugs for standard porosity and permeability measurements, dolomite samples with limited apparent calcite cements were selected. The porosity of these HTD ranges between 1.8 and 13.7% (Fig. 13) with an average of 6.3%. Two samples have exceptionally high permeability values, i.e. 181 and 3785 mD. Permeability values of the other samples range between 0 and 4.4 mD and the average is low (0.6 mD). The correlation between porosity and permeability values of the dolomite

samples is low ( $R = 0.5$ , excluding the outliers) (Fig. 13). When the samples are grouped with regard to their texture, the correlation between porosity and permeability values increases for matrix dolomites to 0.7.

In the field, the highest porosity is systematically observed in the upper part of the HTD body (Fig. 14), where coarse crystalline dolomite is common. These HTD are characterised by large vuggy pores with a porosity of  $\sim 11\%$  based on image analysis (Fig. 10 A and B). Based on standard porosity and permeability analysis the average porosity of the HTD in the upper part of the HTD body is 7.4%, compared to 5.8% in the rest of the HTD body. This small difference is in clear contrast with field observations and is attributed to the sample size. Plugs were used for the petrophysical measurements. Their size is small (2.5 cm diameter,  $\sim 5$  cm length) compared to the size of the existing pores (2–12 cm) that characterise the zebra and coarse crystalline dolomites. In the field, the HTD are cross cut by small fractures and dolomite is known to be a relatively brittle lithology (e.g. Williams and McNamara, 1992). In HTD reservoirs, fracture permeability is often important to explain hydrocarbon flow (Aguilera, 1995). However, when taking plugs, fractured HTD are avoided since plugs will break along the fractures. The porosity and permeability dataset is thus biased, large pores are underrepresented and only the bulk permeability is covered.

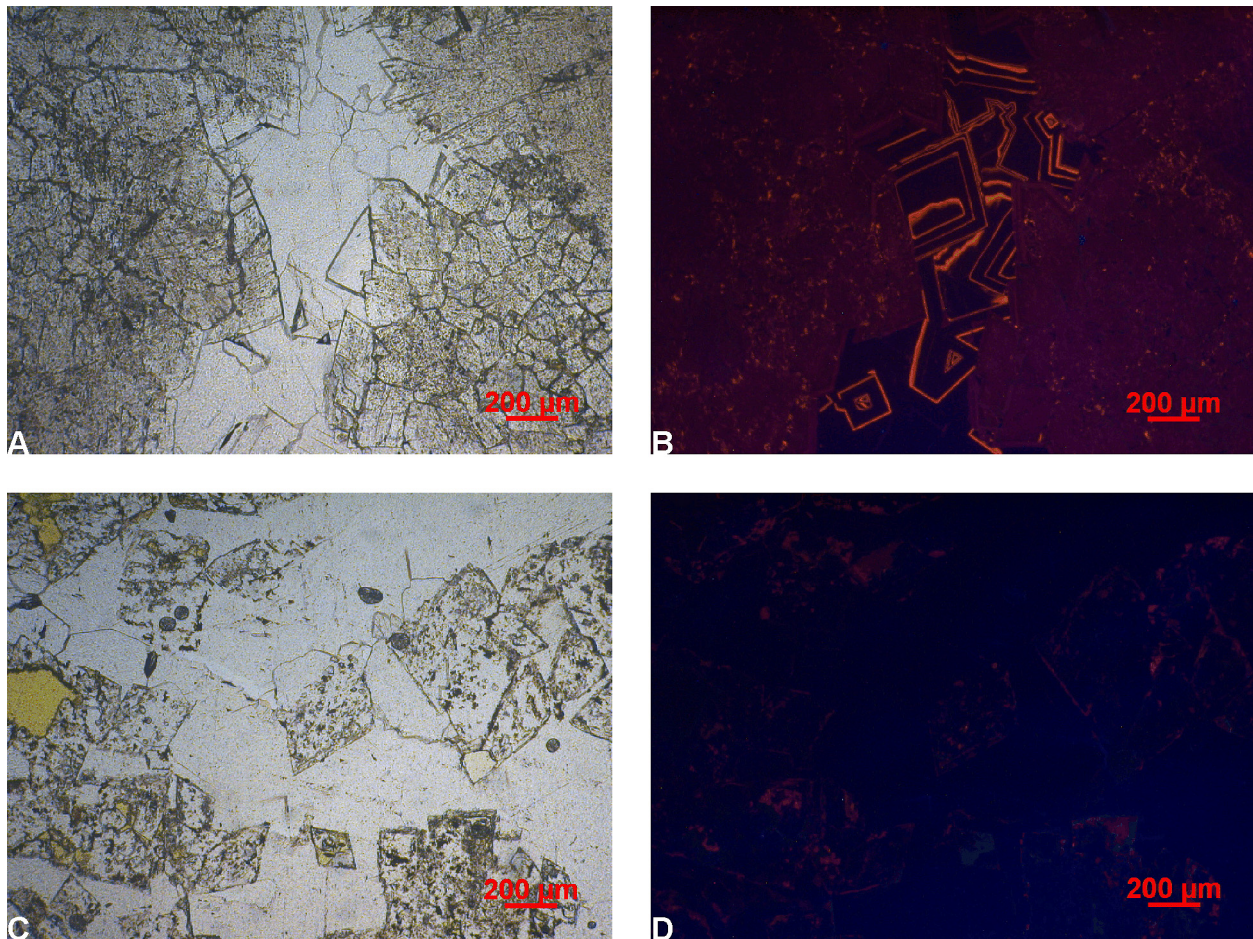
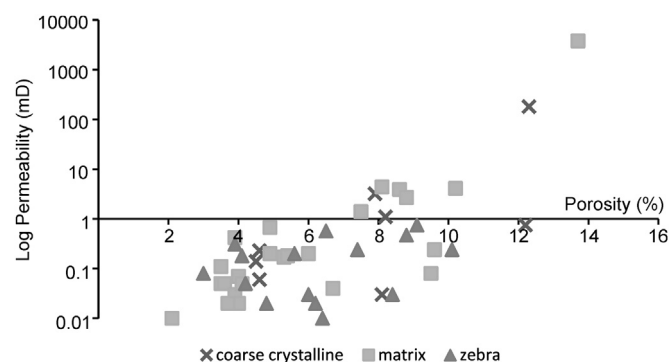


**Figure 12.** A & B. Optical and corresponding cathode luminescence microphotographs. Dolomite crystals contain a lot of impurities, giving them a brown hue. They are corroded along their crystals boundaries. Under cathode luminescence microscopy, this is visible as bright orange luminescent dots. The calcite cement is made up of non- and bright luminescent calcites of the second phase. C & D. Optical and corresponding cathode luminescence microphotographs. The outline of the dolomite crystals can be recognised with normal light. Cathode luminescent microscopy shows that the dolomite crystals lost their characteristic dull red luminescence and are completely replaced by the late calcite. (For interpretation of the references to colour in this figure legend, the reader is referred to the web version of this article.)

### 4.3. Geochemistry

#### 4.3.1. Oxygen and carbon isotope ratios

Stable isotope data ( $\delta^{18}\text{O}$  and  $\delta^{13}\text{C}$ ) of the main diagenetic phases observed at Matienzo are given in Figure 15 and Table 1. The marine stable isotopic signature was retrieved from Price and Hart (1995), Vahrenkamp (1996), Ferreri et al. (1997), Moullade et al. (1998), Grötsch et al. (1998) and Herle et al. (2004). The





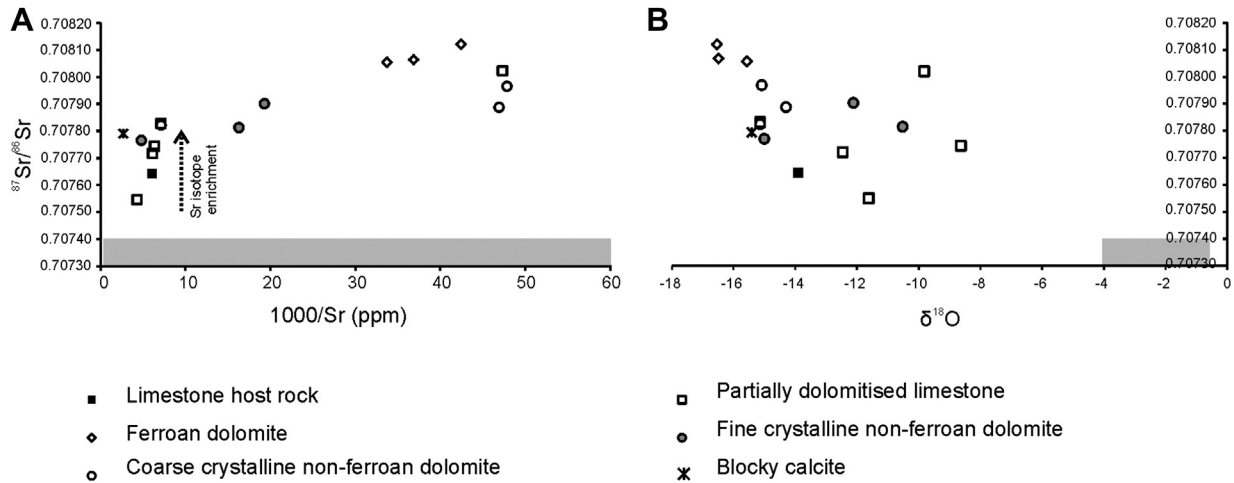


**Figure 16.** Results of Sr isotopic analysis. Marine signatures are indicated by the grey rectangles. A. Cross-plot of  $^{87}\text{Sr}/^{86}\text{Sr}$  and reciprocal Sr concentration. B. Cross-plot of  $^{87}\text{Sr}/^{86}\text{Sr}$  and  $\delta^{18}\text{O}$ -values.

Based on stable isotopic signatures and homogenisation temperatures of both phases, the oxygen isotopic signature of the dolomitising fluid can be calculated. The fractionation equation of Zeng (1999) is suitable for dolomites precipitating in a temperature range as observed in HTD of Matienzo. Based on these calculations, the  $\delta^{18}\text{O}$  value of the parent fluid of the ferroan dolomite varies between  $-2.2$  and  $+8.1\text{‰}$  VSMOW. The parent fluid of the non-ferroan dolomites is characterised by similar values between  $-2.3$  and  $+5.1\text{‰}$  VSMOW.

## 5. Discussion

### 5.1. Controls on HTD distribution and characteristics

No evidence was found in the limestones for any significant porosity at the moment of dolomitisation. Pores were filled by early diagenetic calcite cements and stylolites developed in the host rock before dolomitisation. This might explain why throughout the sections sampled, no relation between precursor limestone facies and dolomite occurrence was found. Grainstones or packstones are

not dolomitised to a greater extent or more frequently than wackestones. As stated by Murray and Lucia (1967) the nature of the original sediment only influences the dolomite distribution to the extent that no secondary changes occurred. At Matienzo, compaction and cementation changed the characteristics of the precursor limestone. As a result, the limestone units were tight and impermeable prior to dolomitisation. Thick limestone beds are efficient barriers to dolomitising fluids. Therefore, bed thickness might be of greater importance than original limestone facies. The influence of the bed thickness on fracture development (i.e. its mechanical behaviour) has been described in literature (Ladeira and Price, 1981; Van Noten and Sintubin, 2010; Jacquemyn et al., 2012). At Matienzo, faults and fractures control the outline of the HTD body and thus represent permeable pathways for diagenetic fluids intruding the host rock. Applying the concepts of mechanical stratigraphy, fracture density is significantly lower in massive beds than in thin beds. In thin beds, dolomitising fluids could thus more easily circulate through a relatively closely spaced fracture network, resulting in a focalised fluid flow, high water–rock interaction and consequently, high potential for pervasive

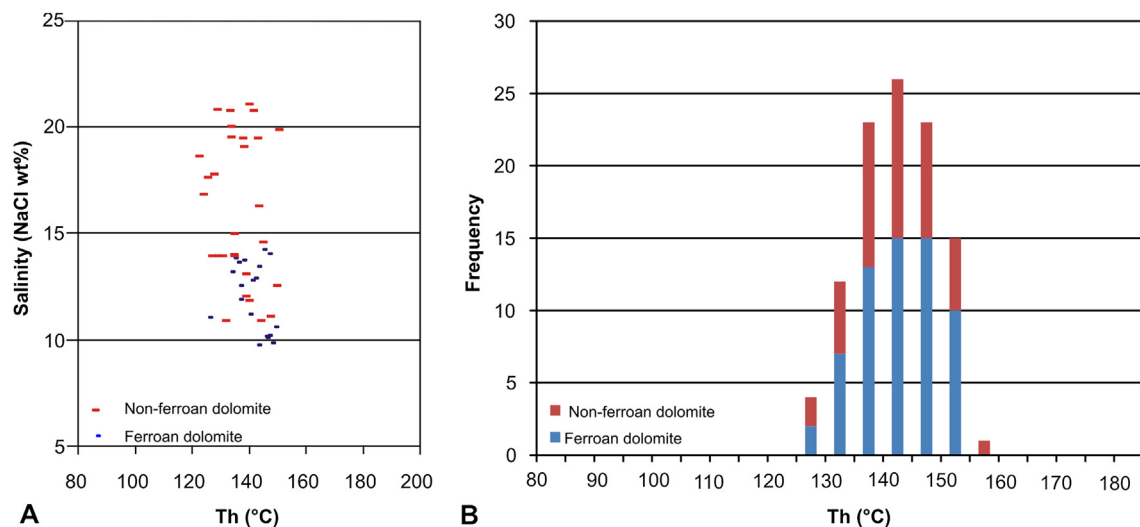


**Figure 17.** Fluid inclusion microthermometry results of primary inclusions of HTD exposed at Matienzo. A. Homogenisation temperature (Th)–Salinity diagram. B. Distribution of homogenization temperatures.

dolomitisation. An additional argument is the fact that the contact between HTD and limestone “stringers” is also controlled by sub-vertical fractures. Moreover, a small subsidiary HTD body cross cuts unit 2 limestones. The orientation of this small, non-stratiform, fracture-related body corresponds to the orientation of joints and dolomite-cemented veins. The dolomitising fluid must thus have been channelled away from the feeder fault (i.e. the fault separating the Central and Eastern Hill) through joints.

The observation of the horst structure at Matienzo indicates that the vertical extent of the HTD body is controlled by the interplay of sub-vertical faults and continuous impermeable units composed of nodular and massive limestone layers. Although a massive limestone unit (MRU) is topping the HTD body at Matienzo, HTD can replace the limestones younger than the MRU when faults cross cut and displace the MRU. Faults are, in general, important conduits for hydrothermal fluids and as long as the fault zone is permeable fluids can migrate through the discontinuity. At the fault's tip, the discontinuity terminates as well as dolomitisation, suggesting that dolomitising fluids could no longer migrate vertically.

A hypothesis involving fluid flow, dolomite saturation and water–rock interaction from the bottom to the top of the HTD body is proposed here to explain the distribution of the HTD types (and related porosity). In the lower part of the HTD body, the dolomitising fluids are highly oversaturated with respect to dolomite. Crystallisation of  $\text{CaMg}(\text{CO}_3)_2$  is therefore fast, which results in fabric-destructive dolomites. Since the fluids are highly oversaturated, dolomite precipitation starts at many nucleation points, which results in small dolomite crystals. When the fluids reach the top of the Matienzo HTD body, their degree of oversaturation with respect to dolomite decreased. Dolomite precipitation starts on fewer nucleation sites and the gradual replacement (dissolution and precipitation) is slower. In addition, not all dissolved components of the host rock are replaced by dolomite phases. Zebra dolomites occur in the central part of the HTD body where the fault separating the Central and Eastern Hill occurs. Zebra dolomite fabrics have been explained in the literature as a result of hydrofracturing of the host rock due to sudden pore-fluid-pressure changes triggered by the focused expulsion of fluid along structural weaknesses (Vandeginste et al., 2005; Davies and Smith, 2006). Considering the spatial relation between zebra dolomite and faults in the HTD body, the zebra dolomites at Matienzo could also be related to overpressured fluids injected along faults. The degree of dolomite saturation could thus account for the distribution of matrix and coarse crystalline HTD in the lower and upper part of the HTD body respectively.

This model can not only be used to explain the distribution of the HTD types, but also supports the distribution of the pore types. Small intercrystalline pores are found in the matrix dolomites that result from efficient replacement of  $\text{CaCO}_3$  and the development of small dolomite crystals in the lower part of the HTD body. Whereas vuggy and moldic pores, characteristic for the coarse crystalline dolomites of the upper part of the HTD body, result from the complete dissolution of  $\text{CaCO}_3$  and partial reprecipitation of  $\text{CaMg}(\text{CO}_3)_2$ .

The observations and data from the Matienzo HTD body permit building a general conceptual model for stratabound HTD bodies (Fig. 18).

1) *Outline of the HTD body.* The HTD body developed roughly parallel to the bedding of the limestone host rock. It is characterised by a limited thickness (80–400 m), but important lateral extent ( $2 \times 4 \text{ km}^2$ ). The lower dolomite-limestone contact is controlled by the strike and dip of the host rock as well as fractures. The upper dolomite-limestone contact is controlled by the interplay

of feeder faults and the presence of a thick impermeable barrier. Where the barrier is cross cut by faults, HTD can be observed above the barrier along these faults until they die out. The lateral distribution did not appear to be controlled by specific limestone facies, though massive limestone layers appear to represent good barriers to dolomitising fluids. Moreover, early diagenetic processes altered the primary characteristics of the limestone host rock. Therefore, bed thickness, controlling fracture spacing, is suggested to be a more important factor than original limestone facies. The relation between bed thickness and fracture density (acting as potential fluid conduits) has been established in literature.

- 2) *Distribution of the HTD types.* Matrix dolomite is generally found in the lower part of the HTD body. In the Central and Eastern Hill, zebra dolomites alternating with matrix dolomite horizons are dominant. Over the entire study area, coarse crystalline dolomite is the main HTD type in the upper part of the HTD body.
- 3) *Distribution of the porosity and permeability of the HTD.* The highest porosity is observed in the upper part (~80 m) of the HTD body. Though large (cm-sized) pores and fracture permeability are not represented in the dataset, the upper part of the HTD body (chiefly consisting of porous coarse crystalline dolomite) is the most interesting in terms of reservoir potential.

## 5.2. Genesis of the HTD

The host rock is cemented by early diagenetic calcite cements. Evidence of a synsedimentary/early diagenetic dolomitisation of the host rock was not observed at Matienzo, neither has a synsedimentary/early diagenetic dolomitisation been described for Aptian–Albian carbonates of the Ramales Platform (García-Mondéjar, 1990; Rosales and Pérez-García, 2010; López-Horgue et al., 2010) or other platforms of the Basque–Cantabrian Basin (Fernández-Mendiola and García-Mondéjar, 1991, 1997; Fernández-Mendiola et al., 1993; Rosales, 1999; Gómez-Pérez et al., 1999). The radiogenic Sr isotopic signature of all samples lies well above the  $^{87}\text{Sr}/^{86}\text{Sr}$  ratio known for Aptian seawater, which ranges between 0.7072 and 0.7074 (McArthur et al., 2001). Therefore, a fluid enriched in radiogenic Sr likely affected the limestones of Matienzo.

The ferroan and non-ferroan dolomites have largely similar geochemical signatures and are therefore discussed together. Both, the ferroan and non-ferroan dolomites are characterised by  $\delta^{13}\text{C}$  values falling within the range of Aptian–Albian marine carbonates. This points to a rock-buffered carbon isotopic signature (Hurley and Lohmann, 1989). The  $\delta^{18}\text{O}$  values, however, are depleted compared to the Aptian–Albian marine carbonates. Sr isotopic signatures are radiogenic for both dolomite phases. Hence, the parent fluid of the dolomites must originate from or have interacted with siliciclastic rocks (Allan and Wiggins, 1993). The dolomitising fluids might have interacted with basement rocks since Pb isotope ratio results from MVT ores of the BCB associated with dolomites indicate that Palaeozoic rocks constitute the Pb source for the galena deposits (Velasco et al., 1994).

Fluid inclusion microthermometry data show that the ferroan and non-ferroan dolomites precipitated from  $\text{H}_2\text{O}$ – $\text{NaCl}$  fluids with a similar homogenisation temperatures, i.e. respectively 126–149 °C and 122–150 °C. However, the salinity range of both phases is different. The first dolomitising fluid is characterised by a narrower salinity range than the salinity of the second dolomitising fluid. Only the latter fluid has salinities higher than 15 eq. wt% NaCl. The wide range of salinity characterising the second dolomitising fluid could be the result of different processes, i.e. 1) mixing of two fluids or 2) an evolution through time of the dolomitising fluid. The

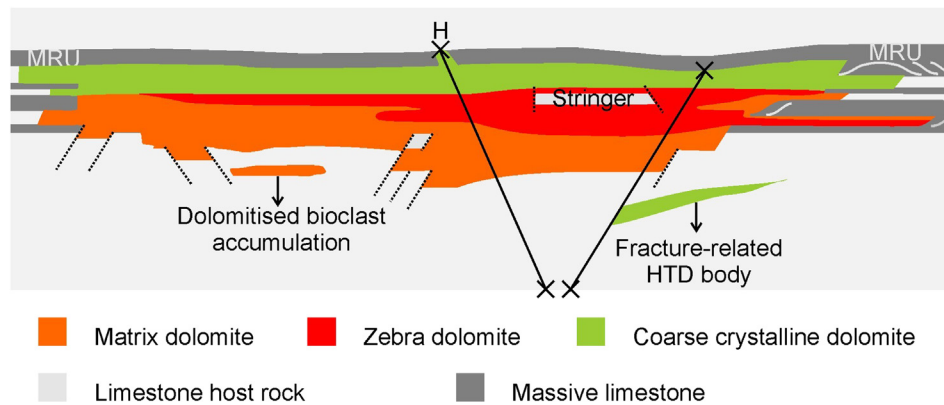


**Figure 18.** Simplified cross-section through the Matienzo HTD body illustrating the general outline of the body controlled by bedding orientation, faults and fractures. Massive beds (dark grey) are impermeable for dolomitising fluids. The MRU seals the top of the HTD body, except where it is cross cut by faults (as observed along the horst structure (H)).

first possibility requires two fluids of the same temperature but different salinity to mix in the subsurface. Nevertheless, fluids with different densities do not easily mix. The second possibility requires the fluid salinity to change through time. This could be the result of faults tapping aquifers with different salinity through time. The high salinity end-member of the non-ferroan dolomites from Matienzo is similar to the salinities inferred from microthermometric analysis of fluid inclusions of ferroan and non-ferroan dolomites from the Ranero area (16–20 eq. wt% NaCl; Dewit, 2012). Therefore, it is suggested that the increase in salinity from ferroan to non-ferroan dolomites at Matienzo is the result of an evolution of the dolomitising fluid through time. During the second dolomitisation phase, the fluid could have been tapped from a similar source as at Ranero.

The Aptian–Albian seawater oxygen isotopic signature is estimated at  $-1\%$  VSMOW by Shackleton and Kennett (1975). For ferroan and non-ferroan dolomites the  $\delta^{18}\text{O}$  values of dolomitising fluids respectively range between  $-2.2$  and  $+8.1\%$  VSMOW and  $-2.3$  and  $+5.3\%$  VSMOW. The positive oxygen isotopic signatures of the dolomitising fluid can be the result of different processes: 1) the fluid interacted at high temperatures with carbonates, resulting in a minor fractionation (Valley, 1986). This can explain the higher isotope ratio values of the dolomitising fluid, but not its high salinity, 2) formation waters enriched in  $^{18}\text{O}$  can be related to smectite-illite conversion and dehydration of clay minerals, which occurs under burial and high temperature conditions (Hitchon and Friedman, 1969; Suchecki and Land, 1983). This process can explain the C–O and Sr isotopic signatures, as well as the elevated Th, but this type of formation waters are generally characterised by lower salinities, 3) the positive values could indicate that the fluid corresponds to modified seawater, possibly evaporated seawater (Hudson, 1977; Land and Prezbindowski, 1981). The third possibility, evaporated seawater, is the most probable considering the geochemical data obtained (high oxygen isotope ratio values and radiogenic Sr isotope ratios) during this study. In addition, crush leach analysis of dolomites from El Mazo – El Moro (located 15 km SE of Matienzo, Fig. 1) of Grandia et al. (2001, 2003) indicates that the salinity of the dolomitising fluid was not achieved by halite dissolution, but originated from a residual fluid remaining after halite precipitation and thus supports the hypothesis that the dolomitising fluid originates from evaporated seawater. This evaporated seawater/residual brine could have formed during the sedimentation of the Keuper deposits of the Basque–Cantabrian Basin, which contain halite, anhydrite and gypsum (Canérot et al., 2005).

Two distinct calcite phases post-date the HTD. The blocky calcite characterised by intense cleavage twins, has depleted  $\delta^{18}\text{O}$  values.

These stable isotope ratio values overlap with those of the ferroan and non-ferroan dolomites. It can thus not be excluded that the stable isotopic signature of this phase is rock-buffered. Only one Sr isotope ratio determination was performed on the blocky calcite cement and the result is similar to the signatures of partly dolomitised host rock and matrix dolomites, which might also support rock-buffering. The honey-coloured calcite, i.e. the second calcite phase that does not possess cleavage twins and post-dates the HTDs, is characterised by a limited range of  $\delta^{18}\text{O}$  values and a large spread in  $\delta^{13}\text{C}$  values. This stable isotopic signature could reflect a meteoric calcite line (Fig. 15; Lohmann, 1988; Muecher et al., 1993). Honey-coloured calcites were also observed at Ranero and interpreted as meteoric cements by Swennen et al. (2012). In addition, meteoric calcites sampled in the Cenozoic basins of Spain (Sanz-Rubio et al., 2001; Arenas et al., 1999; Torres-Ruiz et al., 1994) have similar stable isotopic signatures as those observed in the late honey calcites. Therefore, the honey calcites (and associated dedolomites) are interpreted as meteoric cements.

A relative timing can be attributed to the different diagenetic phases observed at Matienzo. Prior to dolomitisation, the limestone host rock was cemented by early diagenetic calcite cements. Subsequently, bed-parallel stylolites (BPS; Andrews and Railsback, 1996) developed during burial of the Ramales Platform. Prior to a second phase of stylolite development, two dolomitisation phases occurred, i.e. first ferroan and second non-ferroan. Sinistral strike-slip veins cemented by dolomite support a linkage between sinistral strike-slip deformation that occurred during the Late Cretaceous (Vergés et al., 2002) and dolomitisation at Matienzo. Since in the BCB the late Albian is a period of intense tectonic activity (García-Mondéjar et al., 2005) and hydrothermal venting (Agirrezabala, 2009), it is most probable that dolomitisation at Matienzo occurred during the late Albian as was also proposed by López-Horgue et al. (2010) and Swennen et al. (2012). The intense cleavage twins characteristic for the blocky calcite cement indicate calcite cementation pre-dates the final phases of deformation (i.e. Alpine tectonic events). Progressive convergence of the European and Iberian Plate eventually resulted in the emergence of the BCB from the Eocene onwards (Alonso-Zarza et al., 2002). The honey calcite precipitated in the inverted basin due to meteoric diagenesis.

## 6. Conclusions

The large stratabound HTD body of Matienzo developed in Aptian ramp carbonates. It has a tabular shape and the top of the body is controlled by the interplay between feeder fault

terminations and a thick bedded impermeable unit composed of massive limestone beds alternating with nodular limestones. Locally, the impermeable unit, here defined as the MRU, is breached by normal faults. Along these faults, dolomitisation affected the overlying limestones of the MRU.

The lateral contact between the HTD and the host rock is characterised by the presence of dolomite tongues. No obvious relation between the occurrence of dolomite tongues and the original limestone facies has been observed. However, massive limestone beds represent efficient barriers to dolomitising fluids. Therefore, it is suggested that the occurrence of dolomite tongues is related to mechanical stratigraphy rather than to precursor limestone facies.

A systematic distribution of three dolomite types is observed in the stratabound body. Matrix dolomites, characterised by a fine crystalline texture with intercrystalline porosity, are dominant in the lower part of the HTD body. Coarse crystalline dolomites with large vuggy pores are present in the upper 80 m of the HTD body. The middle part of the HTD body is characterised by alternating horizons of zebra and matrix dolomite. Their distribution is explained by the flow of hot dolomitising fluids that ascended along permeable feeder faults. In the lower part of the HTD body, where fluids are highly oversaturated with respect to Mg, fine crystalline, fabric-destructive dolomites are formed. Whereas in the upper part of the HTD body dolomitising fluids are less oversaturated and coarse crystalline dolomites is formed. Due to the lower degree of dolomite saturation, not all dissolved components are replaced by dolomite, which results in high porosity (possibly related to enlarged moldic pores). Zebra dolomites are related to fluid flow focussed along faults occurring in the central part of the HTD body.

Porosity and permeability values of the stratabound HTD are not correlated. Based on field observations, it can be concluded that the upper part of the HTD body, typified by vuggy coarse crystalline dolomites, is the most porous. Conversely, this observation is not supported by the dataset acquired by means of standard porosity and permeability measurements on plug samples. This relates to the relatively small plug diameter (i.e. 2.5 cm) compared to the pore size (i.e. up to 12 cm). Only relatively small pores are thus adequately represented in the acquired dataset. The measured permeability values of the HTD are not high. The HTD body might nonetheless still be interesting in terms of reservoir potential since these permeability values do not cover the fracture permeability. At Matienzo, the upper part of the large stratabound HTD body (~80 m) is suggested to be the most interesting in terms reservoir potential.

No indications for synsedimentary or early diagenetic dolomites have been found in the Matienzo host rocks. After early diagenetic cementation and occlusion of primary pores, bed-parallel stylolites developed. Subsequently, two phases of dolomitisation resulting in ferroan and non-ferroan dolomites, respectively, affected the limestone host rock. Both phases are rather similar from a petrographical and geochemical point of view. The dolomitising fluids were hot (the Th varies between 122 and 150 °C). The parent fluid of the ferroan dolomites has a well-defined salinity range between 9.7 and 14.0 eq. wt% NaCl. The non-ferroan dolomites precipitated from a fluid with a broad salinity range, i.e. between 10.9 and 21.0 eq. wt% NaCl. The high salinity end-member is similar to the salinities inferred for ferroan and non-ferroan dolomites in the area of Ranero. The large salinity range is interpreted as the result of the evolution of the fluid source through time. As the faults continued to develop, different aquifers could have been tapped. Since the salinity of the parent fluid of the dolomites is high, only a highly saline source, such as the Triassic Keuper of the Basque–Cantabrian Basin, containing evaporites can be considered as a viable source.

The Sr isotope results reveal the dolomitising fluid must have interacted with siliclastics.

The limited geochemical data available and possible rock-buffering of the blocky calcite that post-dates dolomite development hamper characterisation of its parent fluid. The second calcite phase post-dating the dolomites is a transparent, honey-coloured calcite. It is characterised by a stable isotopic signature similar to the stable isotopic signature of meteoric calcites sampled in inverted Cenozoic (Miocene) basins Spain. Therefore, the honey calcite precipitated from a meteoric fluid in the inverted Basque–Cantabrian Basin.

## Acknowledgements

This contribution is the result of a collaboration of researchers of the KU Leuven and Statoil A.S.A. The authors would like to thank Statoil A.S.A. for the possibility to publish the data. Julie Dewit benefited of a doctoral grant of the Institute for the Promotion of Innovation through Science and Technology Flanders (IWT). Anneleen Foubert has been funded through FWO–Flanders. Herman Nijs is kindly acknowledged for the careful preparation of the thin-sections and wafers. We would like to thank Prof. M. Joachimsky (University of Erlangen, Germany) for the stable isotope analyses. Kris Latruwe (Ghent University, Belgium) is kindly acknowledged for his help with ICP–QMS and MC–ICPMS analyses. The CT images were kindly provided by Steven Claes (KU Leuven). We would like to thank Paola Ronchi and the anonymous reviewer for their time and valuable comments.

## References

- Agirrezabala, L.M., 2009. Mid-Cretaceous hydrothermal vents and authigenic carbonates in a transform margin, Basque–Cantabrian Basin (Western Pyrenees): a multidisciplinary study. *Sedimentology* 56, 969–996. <http://dx.doi.org/10.1111/j.1365-3091.2008.01013.x>.
- Aguilera, 1995. *Naturally Fractured Reservoirs*. PannWell, Tulsa, Oklahoma, p. 521.
- Allan, J.R., Wiggins, W.D., 1993. Dolomite reservoirs: chemical techniques for evaluating origin and distribution. *Am. Assoc. Pet. Geol. Contin. Educ. Course Notes* 36, 129.
- Alonso, J.L., Pulgar, J.A., García-Ramos, Barba, P., 1996. Tertiary basins and Alpine tectonics in the Cantabrian Mountains (NW Spain). In: Friend, P.F., Dabrio, C. (Eds.), *Tertiary Basins of Spain, the Stratigraphic Record*, vol. 5, pp. 214–227.
- Alonso-Zarza, A.M., Armenteros, I., Braga, J.C., Muñoz, A., Puljate, V., Ramos, E., Aguirre, J., Alonso-Gavilán, G., Arenas, C., Baceta, J.L., Carballeira, J., Calvo, J.P., Corrochano, A., Fornós, J.J., González, A., Luzón, A., Martín, J.M., Pardo, G., Payros, A., Pérez, A., Pomar, Luis, Rodríguez, J.M., Villena, J., 2002. Tertiary. In: Gibbons, W., Moreno, M.T. (Eds.), *The Geology of Spain*, Geological Society, London, pp. 293–334.
- Andrews, L.M., Railsback, L.B., 1996. Controls on stylolite development: morphologic, lithologic and temporal evidence from bedding-parallel and transverse stylolites from the U.S. Appalachians. *J. Geol.* 105, 59–73.
- Arenas, C., Alonso-Zarza, A.M., Pardo, G., 1999. Dedolomitization and other early diagenetic processes in Miocene lacustrine deposits, Ebro Basin (Spain). *Sediment. Geol.* 125, 23–45. [http://dx.doi.org/10.1016/S0037-0738\(98\)00146-8](http://dx.doi.org/10.1016/S0037-0738(98)00146-8).
- Barnaby, R.J., Read, J.F., 1992. Dolomitization of a carbonate platform during late Burial: lower to Middle Cambrian shady dolomite, Virginia Appalachians. *J. Sediment. Res.* 62, 1023–1043.
- Bodnar, R.J., 1993. Revised equation and table for determining the freezing point depression of H<sub>2</sub>O–NaCl solutions. *Geochim. Cosmochim. Acta* 57, 683–684.
- Boillot, G., Malod, J., 1988. The North and North-West Spanish continental margin: a review. *Rev. Soc. Geol. España* 1, 295–316.
- Boni, M., Parete, G., Bechstädt, T., De Vivo, B., Iannace, A., 2000. Hydrothermal dolomites in SW Sardinia (Italy): evidence for a widespread late-Variscan fluid flow event. *Sediment. Geol.* 131, 181–200.
- Braithwaite, C.J.R., Rizzi, G., 1997. The geometry and petrogenesis of hydrothermal dolomites at Navan, Ireland. *Sedimentology* 44, 421–440.
- Burkhard, M., 1993. Calcite twins, their geometry, appearance and significance as stress-strain-markers and indicators. *J. Struct. Geol.* 15, 351–368.
- Canérot, J., Hudec, M.R., Rockenbauch, K., 2005. Mesozoic diapirism in the Pyrenean orogen: salt tectonics on a transform plate boundary. *Am. Assoc. Pet. Geol. Bull.* 89, 211–229.
- Cantrell, D., Swart, P.K., Hagerty, R.M., 2004. Genesis and characterization of dolomite, Arab-D reservoir, Ghawar field, Saudi Arabia. *GeoArabia* 9, 11–36.

- Davies, G.R., Smith Jr., B., 2006. Structurally controlled hydrothermal dolomite reservoir facies: an overview. *Am. Assoc. Pet. Geol. Bull.* 90, 1641–1690. <http://dx.doi.org/10.1306/05220605164>.
- De Muynck, D., Huelga-Suarez, G., Van Heghe, L., Degryse, P., Vanhaecke, F., 2009. Systematic evaluation of a strontium-specific extraction chromatographic resin for obtaining a purified Sr fraction with quantitative recovery from complex and Ca-rich matrices. *J. Anal. Atomic Spectrom.* 24, 1498–1510. <http://dx.doi.org/10.1039/B908645E>.
- Dewit, J., 2012. Genesis and Reservoir Characteristics of Hydrothermal Dolomites (HTD) of the Ramales Platform (Northern Spain) (PhD thesis). KU Leuven, p. 183.
- Dewit, J., Huysmans, M., Muechez, Ph., Hunt, D.W., Thurmond, J.T., Vergés, J., Saura, E., Fernandez, N., Romaine, I., Esestime, P., Swennen, R., 2012. Reservoir characteristics of fault-controlled hydrothermal dolomite bodies: Ramales Platform case study. In: Garland, J., Neilson, J., Whidden, K., Laubach, S. (Eds.), *Special publication of the Geological Society London*, vol. 370, pp. 83–109.
- Dickson, J.A.D., 1966. Carbonate identification and genesis as revealed by staining. *J. Sediment. Pet.* 36 (2), 491–505.
- Dix, G.R., Robinson, G.W., 2003. The geochemical record of hydrothermal mineralization and tectonism inboard the Appalachian orogen: the Ottawa Embayment. *Chem. Geol.* 197, 29–53.
- Fernández-Mendiola, P.A., García-Mondéjar, J., 1990. Mid-Cretaceous palaeogeographical evolution of the central Basque-Cantabrian Basin (Northern Spain). *Palaeogeogr. Palaeoclimatol. Palaeoecol.* 81, 115–126. [http://dx.doi.org/10.1016/0031-0182\(90\)90043-7](http://dx.doi.org/10.1016/0031-0182(90)90043-7).
- Fernández-Mendiola, P.A., García-Mondéjar, J., 1991. Depositional history of Aptian–Albian carbonate platforms: Aitzgorri Massif, northern Spain. *Cretac. Res.* 12, 293–320. [http://dx.doi.org/10.1016/0195-6671\(91\)90038-E](http://dx.doi.org/10.1016/0195-6671(91)90038-E).
- Fernández-Mendiola, P.A., García-Mondéjar, J., 1997. Isolated carbonate platform of Caniego, Spain: a test of the latest Albian Worldwide sea-level changes. *GSA Bull.* 109 (2), 176–194. [http://dx.doi.org/10.1130/0016-7606\(1997\)109<0176:ICPOCS>2.3.CO;2](http://dx.doi.org/10.1130/0016-7606(1997)109<0176:ICPOCS>2.3.CO;2).
- Fernández-Mendiola, P.A., Gómez-Pérez, I., García-Mondéjar, J., 1993. Aptian–Albian carbonate platforms: Central Basque–Cantabrian Basin, northern Spain. In: Toni, T.J.A., Scott, R.W., Masse, J.-P. (Eds.), *Cretaceous Carbonate Platforms*, American Association of Petroleum Geologists, Special Volume, Memoir, 56, pp. 315–324.
- Ferreri, V., Weissert, H., D'Argenio, B., Buonocunto, F.P., 1997. Carbon isotope stratigraphy: a tool for basin to carbonate platform correlation. *Terra Nova* 9, 57–61.
- Gao, G., Land, L.S., Folk, R.L., 1992. Meteoric modifications of early and late dolomitization by basinal fluids, upper Arbuckle Group, Slick Hills, Southwestern Oklahoma. *Am. Assoc. Pet. Geol. Bull.* 76, 1649–1664.
- García-Mondéjar, J., 1989. Strike-slip subsidence of the Basque–Cantabrian Basin of northern Spain and its relationship to Aptian–Albian opening of Bay of Biscay. In: Tankard, A.J., Balkwill, H.R. (Eds.), *European–African Margins*, AAPG Special Volume, vol. M46, pp. 395–409.
- García-Mondéjar, J., 1982. Tectónica sinsedimentaria en el Aptiense y Albiense de la región Vasco-Cantábrica occidental. *Cuad. Geol. Ibér.* 8, 23–36.
- García-Mondéjar, J., 1990. The Aptian–Albian carbonate episode of the Basque–Cantabrian Basin (northern Spain): general characteristics, controls and evolution. In: Tucker, M.E., Wilson, J.L., Crevello, P.D., Sarg, J.F., Read, J.F. (Eds.), *Carbonate Platforms: Facies, Sequences and Evolution*, Special Publication International Association of Sedimentologists, vol. 9, pp. 257–290.
- García-Mondéjar, J., Agirrezabala, L.M., Aranburu, A., Fernández-Mendiola, P.A., Gómez-Pérez, I., López-Horgue, M., Rosales, I., 1996. Aptian–Albian tectonic pattern of the Basque–Cantabrian Basin (northern Spain). *Geol. J.* 31, 13–45.
- García-Mondéjar, J., López-Horgue, M.A., Aranburu, A., Fernández, P.A., 2005. Pulsating subsidence during a rift episode: stratigraphic and tectonic consequences (Aptian–Albian, northern Spain). *Terra Nova* 17, 517–525. <http://dx.doi.org/10.1111/j.1365-3121.2005.00644.x>.
- Gasparini, M., Bechstädt, T., Boni, M., 2006. Massive hydrothermal dolomites in the southwestern Cantabrian Zone (Spain) and their relation to the Late Variscan evolution. *Mar. Pet. Geol.* 23, 543–568.
- Gómez-Pérez, I., Fernández-Mendiola, P.A., García-Mondéjar, J., 1999. Depositional architecture of a rimmed carbonate platform (Albian, Gorbea, western Pyrenees). *Sedimentology* 46, 337–356. <http://dx.doi.org/10.1046/j.1365-3091.1999.00217.x>.
- Gómez, M., Vergés, J., Rianza, C., 2002. Inversion tectonics of the northern margin of the Basque Cantabrian Basin. *Bull. Soc. Geol. Fr.* 173, 449–459. <http://dx.doi.org/10.2113/173.5.449>.
- Grammer, G.M., Harrison, W.B., 2013. Evaluation and Modeling of Stratigraphic Control on the Distribution of Hydrothermal Dolomite Away from Major Fault Planes. RPSEA Final Technical Report, 08123.12.
- Grandia, F., Cardellach, E., Banks, D., Canals, A., 2001. Epigenetic Zn–Pb deposits in Mesozoic basins of the Eastern Iberian Peninsula: evidence for the source of fluids from Na–K–Cl–Br systematic. In: Piestrzynski, et al. (Eds.), *Mineral Deposits of the 21st Century*, pp. 133–136.
- Grandia, F., Canals, A., Cardellach, E., Banks, D.A., Perona, J., 2003. Origin of ore-forming brines in sediment-hosted Zn–Pb deposits of the Basque–Cantabrian Basin, northern Spain. *Econ. Geol.* 98, 1397–1411. <http://dx.doi.org/10.2113/gsecongeo.98.7.1397>.
- Grötsch, J., Billing, I., Vahrenkamp, V., 1998. Carbon-isotope stratigraphy in shallow water carbonates: implications for Cretaceous black-shale deposition. *Sedimentology* 45, 623–634.
- Herle, J.O., Köppler, Friedrich, O., Erlenkeuser, H., Hemleben, C., 2004. High-resolution carbon isotope records of the Aptian to Lower Albian from SE France and the Mazagan Plateau (DSDP Site 545): a stratigraphic tool for paleoceanographic and paleobiologic reconstruction. *Earth Planet. Sci. Lett.* 218, 149–161.
- Hitchon, B., Friedman, I., 1969. Geochemistry and origin of formation waters in western Canada sedimentary basin – 1. Stable isotopes of hydrogen and oxygen. *Geochim. Cosmochim. Acta* 33, 1321–1349.
- Hitzman, M.W., Allan, J.R., Beaty, D.W., 1998. Regional dolomitization of the Waulsortian limestone in southeastern Ireland: evidence of large-scale fluid flow driven by the Hercynian orogeny. *Geology* 26, 547–550.
- Hudson, J.D., 1977. Stable isotopes and limestone lithification. *J. Geol. Soc. Lond.* 133, 637–660.
- Hurley, N.F., Lohmann, K.C., 1989. Diagenesis of Devonian reefal carbonates in the Oscar Range, Canning Basin, western Australia. *J. Sediment. Pet.* 59, 127–146.
- Jacquemyn, C., Swennen, R., Ronchi, P., 2012. Mechanical stratigraphy and (paleo-) karstification of the Murge area (Apulia, southern Italy). In: Garland, J., Neilson, J., Whidden, K., Laubach, S. (Eds.), *Special publication of the Geological Society London*, vol. 370, pp. 169–186.
- Kurz, T.H., Dewit, J., Buckley, S.J., Thurmond, J.B., Hunt, D.W., Swennen, R., 2011. Hyperspectral image analysis of different carbonate lithologies (limestone, karst and hydrothermal dolomites): the Pozalagua Quarry case study (Cantabria, North-west Spain). *Sedimentology* 59, 623–645.
- Ladeira, F.L., Price, N.J., 1981. Relationship between fracture spacing and bed thickness. *J. Struct. Geol.* 13, 179–183. [http://dx.doi.org/10.1016/0191-8141\(81\)90013-4](http://dx.doi.org/10.1016/0191-8141(81)90013-4).
- Land, L.S., Prezbindowski, P.R., 1981. The origin and evolution of saline formation water, Lower Cretaceous carbonates, south-central Texas, U. S. A. *J. Hydrol.* 54, 51–74.
- Lapponi, F., Casini, G., Sharp, I., Blendinger, W., Fernández, N., Romaine, I., Hunt, D., 2011. From outcrop to 3D modelling: a case study of a dolomitized carbonate reservoir, Zagros Mountains, Iran. *Pet. Geosci.* 17, 283–307.
- Lohmann, K.C., 1988. Geochemical patterns of meteoric diagenetic systems and their application to studies of paleokarst. In: James, N.P., Choquette, P.W. (Eds.), *Paleokarst*. Springer-Verlag, New York, NY, pp. 58–80.
- López-Horgue, M., Iriarte, E., Schröder, S., Fernández-Mendiola, P.A., Caline, B., Corneillie, H., Frémont, J., Sudrie, M., Zerti, S., 2010. Structurally controlled hydrothermal dolomites in Albian carbonates of the Asón Valley, Basque–Cantabrian Basin, northern Spain. *Mar. Pet. Geol.* 24 (5), 1069–1092. <http://dx.doi.org/10.1016/j.marpetgeo.2009.10.015>.
- Malone, M.J., Baker, P.A., Burns, S.J., 1996. Hydrothermal dolomitization and recrystallisation of dolomite breccias from the Miocene Monterey Formation, Tepeguet area, California. *J. Sediment. Res.* 66, 976–990.
- Martín-Chivelet, J., Berastegui, X., Rosales, I., Vilas, L., Vera, J.A., Caus, E., Gräfe, K., Mas, R., Puig, C., Segura, M., Robles, S., Floquet, M., Quesada, S., Ruiz-Ortiz, P.A., Fregenal-Martínez, M.A., Salas, R., Arias, C., García, A., Martín-Algarra, A., Melendez, M.N., Chacón, B., Molina, J.M., Sanz, J.L., Castro, J.M., García-Hernández, M., Arenas, B., García-Hidalgo, J., Gil, J., Ortega, F., 2002. Cretaceous. In: Gibbons, W., Moreno, M.T. (Eds.), *The Geology of Spain*, Geological Society, London, pp. 255–292.
- McArthur, J.M., Howarth, R.J., Bailey, T.R., 2001. Strontium isotope Stratigraphy: LOWESS version 3: best fit to the marine Sr-isotope curve for 0–509 Ma and accompanying look-up table for deriving numerical age. *J. Geol.* 109, 155–170. <http://dx.doi.org/10.1086/319243>.
- Morrow, D.W., 1982. Descriptive field classification of sedimentary and diagenetic breccia fabrics in carbonate rocks. *Bull. Can. Pet. Geol.* 30, 227–229.
- Moullade, M., Kuhnt, W., Bergen, J.A., Masse, J.-P., Tronchetti, G., 1998. Correlation of biostratigraphic and stable isotope events in the Aptian historical stratotype of La Bédoule (southeast France). *Earth. Planet. Sci. Lett.* 327, 693–698.
- Muechez, Ph., Peeters, C., Keppens, E., Viaene, W.A., 1993. Stable isotopic composition of paleosols in the lower Viséan of eastern Belgium: evidence of evaporation and soil-gas CO<sub>2</sub>. *Chem. Geol.* 106, 389–396.
- Murray, R.C., Lucia, F.J., 1967. Cause and control of dolomite distribution by rock selectivity. *Geol. Soc. Am. Bull.* 78, 21–36.
- Negra, M.H., Purser, B.H., M'Rabet, A., 1994. Permeability and porosity evolution in dolomitized upper Cretaceous pelagic limestones of Central Tunisia. In: Tucker, M., Zenger, D. (Eds.), *Dolomites: A Volume in Honour of Dolomieu*, Special Publications of the International Association of Sedimentologists, vol. 21, pp. 309–323.
- Nielsen, P., Swennen, R., Muechez, Ph., Keppens, E., 1998. Origin of zebra dolomites south of the Brabant-Wales Massif, Belgium. *Sedimentology* 45, 666–679.
- Price, G.D., Hart, M.B., 1995. Isotopic evidence for early to mid-Cretaceous ocean temperature variability. *Mar. Micropaleontol.* 46, 45–58.
- Rat, 1988. The Basque–Cantabrian Basin between the Iberian and European plates: some facts but still many problems. *Rev. Soc. Geol. Esp.* 1, 3–4.
- Robador Moreno, A., Heredia Carballo, N., Rodríguez Fernández, L.R., Marquinez García, J., 2000. Mapa Geológico de Cantabria. Instituto Geológico y Minero de España.
- Rosales, I., 1999. Controls on carbonate-platform evolution on active fault blocks: the lower Cretaceous Castro Urdiales platform (Aptian–Albian, northern Spain). *J. Sediment. Res.* 69, 447–465. <http://dx.doi.org/10.1306/D4268A09-2B26-11D7-864800102C1865D>.
- Rosales, I., Pérez-García, A., 2010. Porosity development, diagenesis and basin modelling of a Lower Cretaceous (Albian) carbonate platform from northern Spain. In: van Buchem, F.S.P., Gerdes, K.D., Esteban, M. (Eds.), *Mesozoic and Cenozoic Carbonate Systems of the Mediterranean and the Middle East*:

- Stratigraphic and Diagenetic Reference Models, Geological Society, London, Special Publications, vol. 329, pp. 317–342. <http://dx.doi.org/10.1144/SP329.13>.
- Rosenbaum, J., Sheppard, S.M., 1986. An isotopic study of siderites, dolomites and ankerites at high temperatures. *Geochim. Cosmochim. Acta* 50, 1147–1150. [http://dx.doi.org/10.1016/0016-7037\(86\)90396-0](http://dx.doi.org/10.1016/0016-7037(86)90396-0).
- Sanz-Rubio, E., Sánchez-Moral, S., Cañaveras, J.C., Calvo, J.P., Rouchy, J.M., 2001. Calcitization of Mg–Ca carbonate and Ca sulphate deposits in a continental Tertiary basin (Calatayud Basin, NE Spain). *Sediment. Geol.* 140, 123–142. [http://dx.doi.org/10.1016/S0037-0738\(00\)00175-5](http://dx.doi.org/10.1016/S0037-0738(00)00175-5).
- Shah, M.M., Nader, F.H., Dewit, J., Swennen, R., Garcia, D., 2010. Fault-related hydrothermal dolomites in Cretaceous carbonates (Cantabria, northern Spain). *Bull. Soc. Géol. Fr.* 181, 389–405. <http://dx.doi.org/10.2113/gssgfbull.181.4.391>.
- Shah, M.M., Nader, F.H., Garcia, D., Swennen, R., Ellam, R., 2012. Hydrothermal dolomites in the early Albian (Cretaceous) platform carbonates (NW Spain): nature and origin of dolomites and dolomitising fluids, oil. *Gas. Sci. Technol.* 67, 97–122.
- Shackleton, N.J., Kennett, J.P., 1975. DSDP Reports and Publications. Paleotemperature History of the Cenozoic and the Initiation of Antarctic Glaciation Oxygen and Carbon Isotope Analyses in DSDP Sites, vol. XXIX, pp. 743–755.
- Sharp, I., Gillespie, P., Morsalnezhad, D., Taberner, C., Karpuz, R., Vergés, J., Horbury, A., Pickard, N., Garland, J., Hunt, D., 2010. Stratigraphic architecture and fracture controlled dolomitization of the Cretaceous Khami and Bangestan groups: an outcrop case study, Zargos Mountains, Iran. In: van Buchem, F.S.P., Gerdes, K.D., Esteban, M. (Eds.), *Mesozoic and Cenozoic Carbonate Systems of the Mediterranean and the Middle East: Stratigraphic and Diagenetic Reference Models*, Geological Society, London, Special Publication, vol. 239, pp. 343–396. <http://dx.doi.org/10.1144/SP329.14>.
- Sibuet, J.-C., Srivivasta, S.P., Spakman, W., 2004. Pyrenean orogeny and plate kinematics. *J. Geophys. Res.* 109 (B08104), 18. <http://dx.doi.org/10.1029/2003JB002514>.
- Suchocki, R.F., Land, L.S., 1983. Isotopic geochemistry of burial metamorphosed volcanogenic sediments, Great Valley sequence, northern California. *Geochim. Cosmochim. Acta* 47, 1487–1499.
- Sun, Q., 1995. Dolomite reservoirs: porosity evolution and reservoir characteristics. *Am. Assoc. Pet. Geol. Bull.* 79, 186–204.
- Swennen, R., Dewit, J., Fierens, E., Muechez, Ph., Shah, M., Nader, F.H., Hunt, D., 2012. Multiple dolomitisation events along the Ranero fault (Pozalagua Quarry, Basque–Cantabrian Basin): episodic earthquake activity. *Sedimentology* 59, 1345–1374. <http://dx.doi.org/10.1111/j.1365-3091.2011.01309.x>.
- Thirlwall, M.F., 1991. Long-term reproducibility of multicollector Sr and Nd isotope ratio analysis. *Chem. Geol.* 94, 85–104. [http://dx.doi.org/10.1016/0168-9622\(91\)90002-E](http://dx.doi.org/10.1016/0168-9622(91)90002-E).
- Torres-Ruiz, J., López-Galindo, A., González-López, Delgado, A., 1994. Geochemistry of Spanish sepiolite-palygorskite deposits: genetic considerations base don trace elements and isotopes. *Chem. Geol.* 112, 221–245. [http://dx.doi.org/10.1016/0009-2541\(94\)900026-4](http://dx.doi.org/10.1016/0009-2541(94)900026-4).
- Vahrenkamp, V., 1996. Carbon isotope stratigraphy of the Kharaiib and Shuaiba FM: implications for the Early Cretaceous Evolution of the Arabian Gulf. *Am. Assoc. Pet. Geol. Bull.* 80, 647–662.
- Valley, J.W., 1986. Stable isotope geochemistry of metamorphic rocks. In: Valley, J.W., Taylor, H.P., O'Neil, J.R. (Eds.), *Stable Isotopes in High Temperature Geological Processes, Reviews in Mineralogy*, vol. 16, pp. 445–489.
- Vandeginste, V., Swennen, R., Gleeson, S.A., Ellam, R., Osadetz, K., Roure, F., 2005. Zebra dolomitization as a result of focalized fluid flow in the Rocky Mountains Fold and Thrust Belt. *Sedimentology* 52, 1067–1095.
- Vanhaecke, F., De Wannemacker, G., Moens, L., Hertogen, J., 1999. The determination of strontium isotope ratios by means of quadrupolebased ICP-mass spectrometry: a geochronological case study. *J. Anal. Atomic Spectrom.* 14, 1691–1696. <http://dx.doi.org/10.1039/A905184H>.
- Van Noten, K., Sintubin, M., 2010. Linear to non-linear relationship between vein spacing and layer thickness in centimetre- to decimetre-scale siliciclastic multilayers from the high-Ardenne slate belt (Belgium, Germany). *J. Struct. Geol.* 32, 377–391. <http://dx.doi.org/10.1016/j.jsg.2010.01.011>.
- Velasco, F., Herrero, J.M., Gil, P.P., Alvarez, L., Yusta, I., 1994. Mississippi Valley-Type, Sedex, and iron deposits in the lower Cretaceous rocks of the Basque–Cantabrian Basin, northern Spain. In: Fontboté, Boni, M. (Ed.), *Sediment-hosted Zn–Pb Ores*, Geological Society, London, Special Publications, vol. 10, pp. 246–270.
- Vergés, J., Fernández, M., Martínez, A., 2002. The Pyrenean orogeny: pre-, syn- and post-collisional evolution. In: Rosenbaum, G., Lister, G. (Eds.), *Reconstruction of the Evolution of the Alpine-Himalayan Orogen*, *J. Virtual Explor.* 8, 55–74.
- Wachter, E., Hayes, J.M., 1985. Exchange of oxygen isotopes in carbon-dioxide - phosphoric acid systems. *Chem. Geol.* 52, 365–374. [http://dx.doi.org/10.1016/0168-9622\(85\)90046-6](http://dx.doi.org/10.1016/0168-9622(85)90046-6).
- Warren, J., 2000. Dolomite: occurrence, evolution and economically important associations. *Earth-Sci. Rev.* 52, 1–81.
- Wilkinson, J.J., 2003. On diagenesis, dolomitisation and mineralisation in the Irish Zn–Pb orefield. *Miner. Deposita* 38, 968–983.
- Williams, D.M., McNamara, K., 1992. Limestone to dolomite to dedolomite conversion and its effect on rock strength; a case study. *Q. J. Eng. Geol. Hydrogeol.* 25, 131–135.
- Zeng, Y.F., 1999. Oxygen isotope fractionation in carbonate and sulphate minerals. *Geochem. J.* 33, 109–126.